Influence of sampling approaches on physical and geochemical analysis of aeolian dust in source regions

Von Holdt, J.R.C.[1], Eckardt, F.D. [1], Baddock, M.C.[2], Hipondoka, M.H.T.[3], Wiggs, G.F.S.[4]

[1]Department of Environmental and Geographical Science, University of Cape Town, Private Bag X3, Rondebosch, Cape Town 7701, South Africa

[2]Geography and Environment, Loughborough University, Loughborough, Leicestershire, UK LE11 3TU

[3]Department of Geography, History, Environmental Studies and Tourism Management, University of Namibia, 340 Mandume Ndemufayo Ave, Pionierspark, Windhoek, Namibia

[4]School of Geography and the Environment, Oxford University Centre for the Environment, University of Oxford, Oxford, UK OX1 3QY

Keywords: Mineral dust, sampling, auto-SEM, PI-SWERL, BSNE; individual particle analysis

Abstract

The characterisation of mineral dust at emission sources is essential for quantifying the wider-scale environmental impacts dust has, as well as improving its incorporation in modelling. Methods of sampling sediments at these source areas for the purposes of dust characterisation are varied and can produce different representations of emitted dust. This study systematically compared dust characterisations from three established approaches for estimating dust emission potential, namely: Big Spring Number Eight (BSNE) traps, a Portable In-situ Wind Erosion Laboratory (PI-SWERL) wind tunnel, and bulk surface sampling, at a known Namib Desert dust source. Individual particle analysis by auto-SEM (QEMSCAN) allowed comparison of size, shape, mineralogy and elemental composition at micrometre-scale for samples from the three approaches. BSNE samples consisted of a lower proportion of fine

sediment (<20 μm particle diameter) than PI-SWERL-derived samples, with this performance possibly influenced by atmospheric humidity. In comparison, PI-SWERL characterised the dust with relatively fewer particles between 63-100 μm, a fraction that was more evident in both the BSNE-derived and surface sediments. The reduced representation of this coarser fraction resulted in appreciable differences in particle shape and mineralogic characteristics compared to BSNE and surface-derived samples. The different representations by the three methods return variable dust characteristics at source across fundamental properties of particle size, shape and mineralogy. Awareness of the different representations of dust caused by sampling technique remains essential for the appropriate physical and geochemical characterisation of aeolian dust and highlights how standardised techniques are important for meaningful comparisons, while methods to achieve accurate characterisation remain a priority for the discipline.

Introduction

Mineral aerosols generated from desert regions provide nutrients to both marine and terrestrial ecosystems and affect climate (e.g. Jickells et al., 2005; Knippertz and Stuut, 2014; McTainsh and Strong, 2007; Shao et al., 2011a). The determination of the physio-chemical properties of surface sediments at emission source areas and suspended aeolian dust itself provides valuable information regarding the provenance and evolution of dust from emission to deposition. The size, mineralogy and shape of the dust particles are crucial characteristics for understanding the effects that the particles have, including the transformations they undergo from source, during transport to the point of deposition. These fundamental characteristics are dependent in the first place on the sediments at the source of emission, as influenced by the geology and geomorphology of the landscape, as well as the active weathering regime. Because dust composition depends heavily on source sediments, the sampling and measurement approaches

52 employed to characterise dust represent a crucial consideration and ideally, varied approaches
53 should yield comparable results. The correct measurement (and subsequent parameterisation)
54 of dust characteristics at source is important for improving our understanding of emissions
55 processes, as well as the modelling of the full dust cycle and assessing the potential downwind
56 impacts of the emitted dust (Kok et al., 2012; Mahowald et al., 2014).

57 Particle size is a primary determinant of the environmental impact of mineral dust due to the
58 fact it has a significant initial control on sediment erodibility and subsequently the duration and
59 distance of transport. However, the representation and measurement of the size distribution of
60 aeolian dust samples remains a challenge (Formenti et al., 2011; Kok et al., 2011a). The
61 particle-size distribution (PSD) in source sediments influences how the suspended dust PSD
62 changes in the atmosphere and consequently how the emission and transport processes are
63 modelled (Mahowald et al., 2014; Shao et al., 2011b; Nousiainen, 2009). The PSD of emitted
64 dust is generally thought to depend on the source soil properties, such as parent soil particle
65 size distribution, and also wind speed (Kok et al., 2011a, 2011b). However, based on empirical
66 observations, Mahowald et al. (2014) contended that this applies only to the >5 μm size fraction
67 and that the size distribution of the emitted dust <5 μm is independent of soil PSD and wind
68 speed. The coarser dust particles (>5 μm) constitute a substantial fraction of the vertical dust
69 flux and despite their size, are recognised as having the potential to travel far from the emission
70 source (Ryder et al., 2013). For example, van der Does et al. (2016) recently found modal grain
71 sizes between 4 and 32 μm along a transect in the Atlantic Ocean up to 4400 km from the north
72 African source region. Their findings provide novel evidence that the transport of coarser dust
73 fractions may be significant over much larger distances than previously considered. Such
74 findings are based on measurement of deposited dust, but field-based methods to sample and
75 measure aeolian dust at emission sources are required to elucidate controls on erodibility and
76 characteristics of dust at uplift.

77 The mineral and elemental composition of aerosols are important characteristics that will
78 influence the types of interaction that take place between dust particles and the atmosphere,
79 ocean and terrestrial environments (Formenti et al., 2011; Mahowald et al., 2011). For example,
80 dust provides important nutrients, such as Fe, that affect the biogeochemical cycles of the ocean
81 (Jickells and Moore, 2015; Mahowald et al., 2005), with the quantity and bioavailability of Fe
82 fundamentally determined by the mineralogy of the particles (Journet et al., 2008). Minerals
83 have different refractive indices and so mineral composition, in combination with particle size
84 and shape, also influences the radiative properties of the aerosols. This has a direct influence
85 on the solar and infra-red radiation absorption properties of the dust (Claquin et al., 1999;
86 Kalashnikova and Sokolik, 2002; Nousiainen, 2009). Mineralogy is also important for the
87 indirect effect of dust on the radiative budget, such as Ca-bearing minerals acting as cloud
88 condensation and ice nuclei (Atkinson et al., 2013; Laskin et al., 2005; Sullivan et al., 2009).
89 The mineral and chemical compositions of aeolian dust are also recognised to be useful for
90 investigating sediment provenance (Yang et al., 2007; Muhs et al., 2014). Dust constitutes a
91 combination of various minerals including clays, quartz, carbonates, feldspars, sulphates and
92 iron oxides (Sokolik and Toon, 1999), with the composition and proportions of the minerals in
93 emitted dust being dependent on the mineralogy of the source soil (Claquin et al., 1999; Journet
94 et al., 2014; Nickovich et al., 2012). With its environmental impact influenced by variable
95 mineralogy, accurate characterisation of emitted dust at sources is essential for improving
96 predictions regarding the complex environmental role dust plays in the Earth system.

97 Particle shape is also recognised to affect the settling or sedimentation velocity of dust, with
98 flat particles expected to travel further than spherical particles for a given velocity (Formenti
99 et al., 2011; Ginoux, 2003). Friese et al. (2016) recorded particle sizes up to 250 μm for Saharan
100 windblown sediment sampled 150 km off-shore and related this to the capacity of platy-shaped
101 mica particles to travel further distances than a spherical particle of equivalent size. The effect

of non-sphericity on sedimentation velocity becomes particularly pronounced in combination with particle size and density. Furthermore, particle shape can also influence the light scattering abilities of the aerosols. Such properties are heavily dependent on the sphericity of the particles (Kalashnikova and Sokolik, 2002) and this is important because the characterisation of dust particle sizes often assumes a strong sphericity in particle shape (Mahowald et al., 2014). The shape factor is also understood to have important implications for determination of radiative forcing by dust and its effect on climate, and for radiances detected in remote sensing applications (Formenti et al., 2011; Nousiainen, 2009).

A variety of methods have been employed to sample the windblown or wind-erodible sediment at emission sources. These include windblown sediment samplers on-site or downwind of dust sources, including passive samplers such as Big Spring Number Eight (BSNEs) and Modified Wilson and Cooke samplers (MWACs) (e.g. Dansie et al., 2017a; Fryrear, 1986; Gillette et al., 1997; Goossens and Buck, 2012; Hahnenberger and Perry., 2015; Warren et al., 2007, Waza et al., 2019), resuspension chambers (Engelbrecht et al., 2016), wind tunnel measurements and sampling (e.g. Lafon et al., 2006; Van Pelt et al., 2017; Wang et al., 2015; Wang et al., 2017), and samples of the wind-erodible fraction of surface sediments as a proxy for emitted dust (e.g. Bhattachan et al., 2015; Dansie et al., 2017b; Reynolds et al., 2007; von Holdt and Eckardt, 2017; Wang et al., 2005). Among the different methods, the Portable In Situ Wind Erosion Laboratory (PI-SWERL) has emerged as a standardized approach for measuring emission potential, allowing comparable estimations of dust flux potential from different surfaces, capturing emission variability through its ability to quickly and easily undertake numerous replicable measurements (e.g. Etyemezian et al. 2007; Sweeney et al., 2008; Sweeney et al., 2011; von Holdt et al., 2019, Cui et al., 2019). The sampling of sediments from the PI-SWERL exhaust has only been done in a limited number of studies, such as Vickery and Eckardt, (2020) and Wang et al., (2015). This range of field techniques provides the means to obtain

fundamental information about the characteristics of windblown or wind-erodible sediment from emission source areas. However, the variable design, efficiencies and biases across different methods can potentially result in the sampling and measurement of varying fractions with different proportions of particle sizes (Goossens and Buck, 2012). For example, BSNE samplers have been shown to exhibit an inefficiency at trapping fine particles (<10 μm) (Shao et al., 1993; Sharrat et al., 2007; Sow et al., 2006), leading to an overrepresentation of coarser dust fractions. Such influences on the sediment sampled could lead to different interpretations of the physicochemical characteristics of the emitted dust, stemming from the sampling approach.

Analysis of the size and mineralogy of windblown and surface sediments at source has been performed in many studies (e.g. Formenti et al., 2003; Hojati et al., 2012; Rashki et al., 2013). The particle size distributions can be determined by several methods including the measurement of the geometric diameter by Coulter counter, imaging techniques such as optical microscopy or optical diameters by laser diffraction (Mahowald et al., 2014). The mineralogy of dust has been determined extensively on a semi-quantitative basis with X-ray diffraction (XRD) for the major mineral phases (e.g. Falkovich et al., 2001; Shi et al., 2005) and the elemental composition quantitatively with X-ray fluorescence (XRF) spectrometry or inductively coupled plasma atomic emission spectroscopy/mass spectroscopy (ICP-AES/ICP-MS) (e.g. Reheis et al., 2009; Trapp et al., 2010, Zhang et al., 2001; Zhuang et al., 2001). These analyses can, however, only discriminate between particle sizes based on physically separated fractions, such as by sieving. Individual particle analysis has been performed with scanning and transmission electron microscopy (SEM and TEM) in combination with energy-dispersive X-ray microanalysis to determine composition and shape (e.g. Engelbrecht et al., 2009; Jeong et al., 2008), but these techniques generally involve a limited number of particles which are not necessarily representative of the sampled dust. The development of automated SEM

(computer-controlled) for individual particle analysis enables the determination of the size, composition and shape of a statistically significant number of individual particles (e.g. Deboudt et al., 2010; Engelbrecht et al., 2016; Kandler et al., 2007, 2009; Krueger et al., 2003; Reid et al., 2003; Speirs et al., 2008, Waza et al., 2019). Computer-controlled SEM analysis of sampled sediment offers the ability to enable a detailed comparison of sampled sediment for comparative purposes.

This study compared the characterisation of aeolian dust at an emissions source area in the Namib Desert using three common sampling approaches as used in the quantification of dust emission by flux or in estimating the potential for emission. These were bulk surface-sediment sampling, windblown dust collected in BSNE traps and, finally, dust samples obtained from operation of a PI-SWERL wind tunnel. A high-resolution auto-SEM (QEMSCAN) analysis was used to compare the size, mineral composition, and shape of individual particles sampled with each method. The detail of our study reveals that these sampling techniques can result in the collection of different fractions of the dust, highlighting the value of a consensus approach that comprises all three sampling techniques, and allows for future studies to evaluate potential biases in sediment analysis dependent upon applied sampling techniques.

Regional setting

The ephemeral river valleys in the Namib Desert are major dust sources in southern Africa (Fig 1a), with large plumes visible on satellite imagery as dust is transported over the ocean during strong autumn and winter easterly winds (Vickery et al., 2013; Dansie et al., 2017b). The Huab river catchment, one such dust bearing system, is located in a basement of the Upper Proterozoic to Cambrian Damara Sequence (Fig 1b), overlain by Carboniferous to Permian Karoo Supergroup sediments of fluvio-lacustrine and fluvio-marine origin (Jerram et al., 2000). An angular unconformity, with a gap of up to 120 Ma, exists between the Karoo Supergroup

and the deposition of the Etendeka Group (c. 133 Ma) which marks the separation of Africa from South America. This group includes the fluvial and aeolian units of the Cretaceous Etjo Formation, intruded and covered by the volcanic flood basalts of the Etendeka Igneous Province (Jerram et al., 1999). The Damara Sequence locally provides schists, granites and marbles. The Karoo Supergroup adds shales, siltstones and mudstones and the Etendeka contribute basalt, andesite as well as sandstone of the Etjo formation.

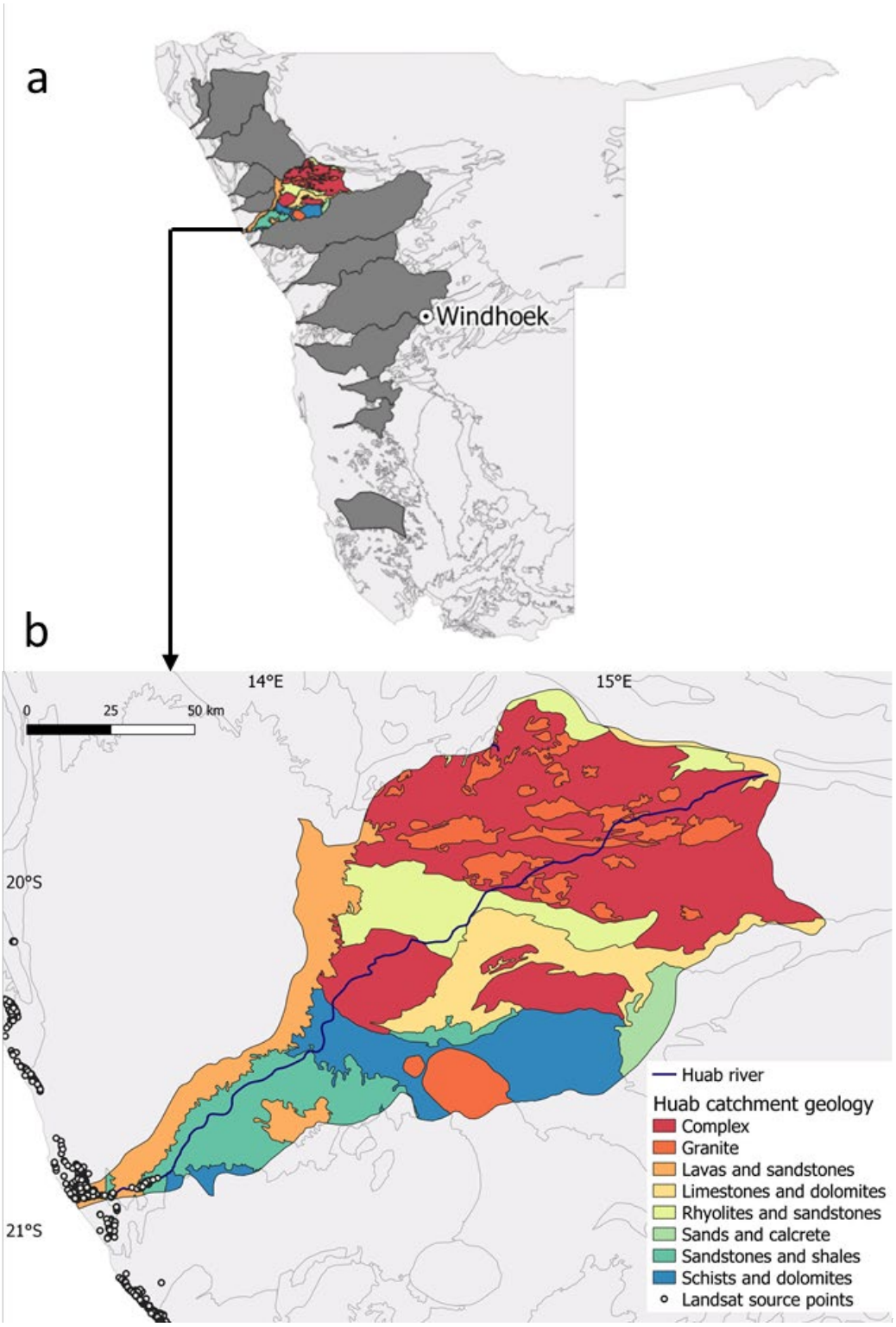

Figure 1: a) The location of the Huab study catchment and other ephemeral river catchments in Namibia, b) Geology of the Huab catchment in terms of Complex, Group and main rock types.

Also indicated are point sources of dust emission as determined by the identification of the upwind points of dust plumes in Landsat imagery (see von Holdt et al., 2017)

The Huab is one of the most actively dust emitting ephemeral river systems in Namibia according to analyses of remote sensing, with consistent dust emission sites situated within the river at an upstream section associated with fluvial silt terraces, and at downstream stages where there are fine sediment deltaic deposits, as well as from the pans situated to the north and south (Vickery et al., 2013; von Holdt et al., 2017). Dust emission tests with the PI-SWERL confirmed the high emission potential of the Holocene fluvial silt terraces (von Holdt et al., 2017), with no flood events recorded on these raised fill sediments for the last c.600 years from OSL chronology performed by Thomas et al. (2017). In addition, Dansie et al. (2017a) further confirmed the emission potential of the alluvial sediments in this system with ground-based measurements from seven stations situated throughout the river valley. These measurements included monitoring of dust concentrations through a combination of a DustTrak DRX aerosol monitor and meteorological conditions from an automatic weather station. In addition, windblown sediment samples were collected with a tower of BSNE traps. Dansie et al. (2017a, b) highlighted the ocean fertilisation potential of the surface and windblown sediments collected with the BSNEs from the Huab with elevated levels of bioavailable Fe, P and N. von Holdt et al. (2019) quantified the emission potential of the landforms of this system with a PI-SWERL wind tunnel, identifying the nebkhas and paleo silt terraces with available mobile sand as preferential surfaces for emission.

Methods

Field sites and measurements

Dust emission measurements with a Portable In-Situ Wind ERosion Lab (PI-SWERL) wind tunnel (Etyemezian, 2007, Sweeney et al., 2008, 2011, Goossens and Buck, 2009, Bacon et al., 2011, von Holdt et al., 2017, Cui et al., 2019) were carried out at seven sites within the Huab River system, including the Huab Pan and the adjacent gravel plain. These sites were chosen based on the remote sensing analysis of dust sources by Vickery et al. (2013) and von Holdt et al. (2017; 2019). The measurement sites included the main geomorphic units within the dust-producing area of the river system, which included the valley fill and delta terraces (four sites: Huab 1, 2, 4, 7), the river channel itself (one site: Huab 3), gravel plain (one site: Huab 5) and the Huab Pan to the north of the river (one site: Huab 6) (Figure 2). All PI-SWERL measurements were carried out as a 5-minute constant rotation test, building up to 3300 rpm (with 120 seconds to reach target rpm) followed by a runtime of 180 s at the maximum rotation speed. The friction velocity applied by the PiSwerl to the surface (3300 rpm = u^* of 0.55 - 0.58 ms^{-1}) equated to a wind speed of approximately 8 ms^{-1} at 10 m height when adjusted for surface roughness (Etyemezian et al., 2014) and represented a threshold at which saltation was initiated (Fryberger, 1979; Stout, 2007). The analysis of remote sensing data for dust emission in the Namib confirms the appropriateness of this threshold friction velocity for dust emission (von Holdt et al., 2017). A constant rotation speed was used to simplify the variables selected for this analysis. The PI-SWERL was used for experiments at seven sites with 5 to 10 replicate measurements undertaken spaced at 1 m apart on a transect line (Figure 3).

Samples of dust from the PI-SWERL exhaust were taken from two measurement runs that produced appreciable dust emissions and were collected by sealing a plastic bag over the instrument's exhaust to capture emitted dust over the full duration of the test run. These runs were situated on the river valley and delta fill terraces (Huab East and Huab West on Figure

2). For the bulk surface sampling approach, soil samples of approximately 200 g were taken adjacent to the position of each PI-SWERL run and consisted of a scrape of the top 0.02 m of soil, ensuring that the surface type and sediment remained consistent with the wind tunnel-tested surface. The two sites (Huab East and West) are situated 17 km from each other in a section of the river where the transport of sediments by floods generated in the highlands drives the supply of material that can be entrained by the wind. As a result, the sediments at the two study sites are predominantly derived from the same geology found in the upper catchment.

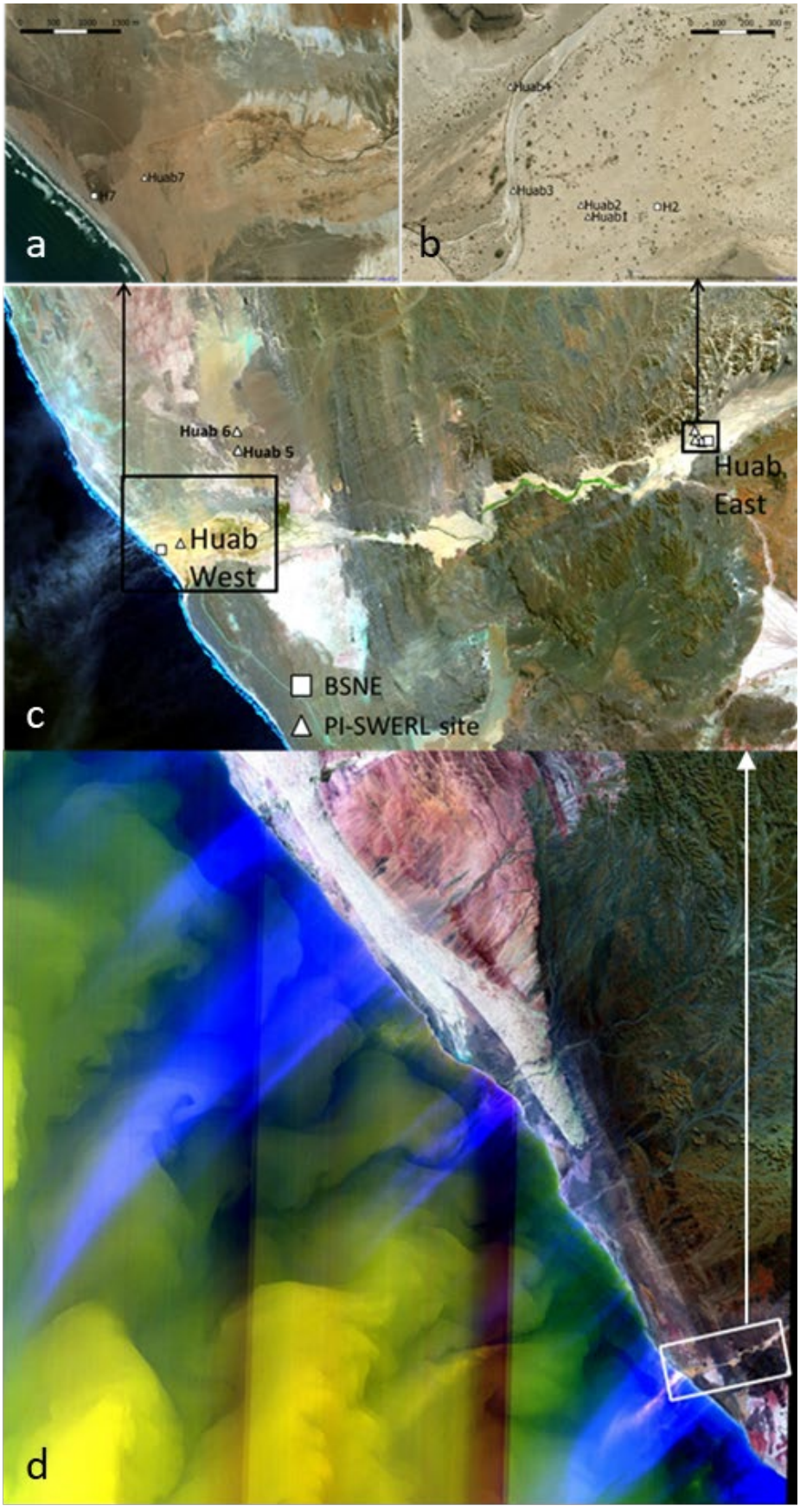
a
Huab7
H7
b
Huab4
Huab3
Huab2
Huab1
H2
c
Huab 6
Huab 5
Huab West
Huab East
BSNE
PI-SWERL site
d

239

Figure 2 Test sites in the Huab River system. PI-SWERL test sites are marked with triangles from Huab 1-7 in panel a, b and c and are located in the following landform types: Huab 1,2, 4, 7 on valley/delta fill terraces, Huab 3 within the active channel, Huab 5 on the gravel plain and Huab 6 on Huab Pan. BSNE samples were obtained from sites marked with squares at Huab West (H7) and Huab East (H2) in panels a, b and c. This study focused on the two sites labelled Huab West and Huab East. Top images (panel a and b) obtained from Bing Aerial imagery (Microsoft Bing, 2017). The image in panel c is the Landsat 8 false colour image (bands 7,5,3) for 21 July 2013. The bottom image (panel d) shows the north-east Bergwind event captured by Landsat 8 on 21 July 2013 resulting in significant dust plumes emanating from the dry river valleys in blue. Stacked image created with a shortwave infrared band (7) and the two thermal infrared bands (10,11). This event occurred while the BSNEs were deployed.

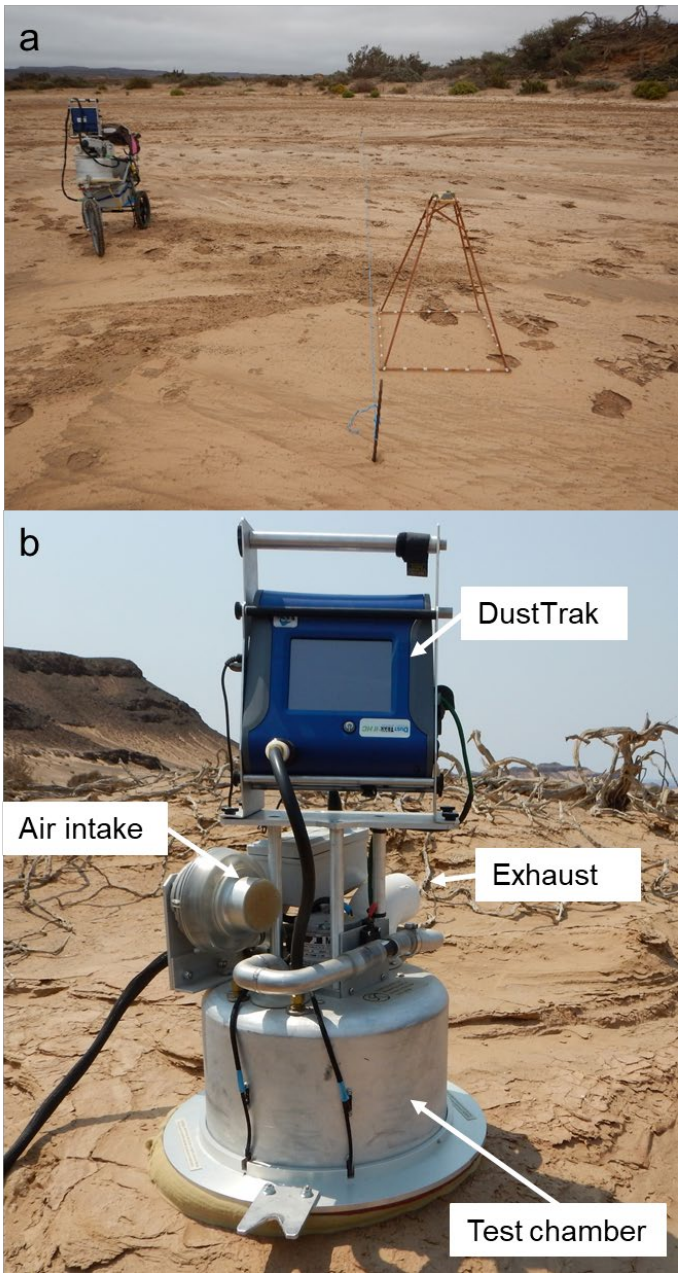

Figure 3 (a) PI-SWERL experimentation site within the Huab active channel (Huab 3). Here, each site consisted of a minimum of 5 runs along a transect (marked with blue rope). PI-SWERL wind tunnel on its buggy on the left and pyramid frame for taking surface photos also shown. (b) PI-SWERL instrument deployed on the surface, showing exhaust outlet which was sampled during test runs.

For the final sampling procedure, a tower with BSNE samplers was erected within each of the East and West sites (squares in Figure 2). The BSNE samplers are wedge-shaped traps based on the design by Fryrear (1986) and samples were obtained from a trap placed at 0.89 m (Table 1). For the comparison between sampling methods done as part of this study, the PI-SWERL and surface samples in proximity to the BSNE towers were selected for analysis (Table 1).

Laboratory preparation of the collected sediment samples saw the samples from the surface, one PI-SWERL sample and the BSNEs from Huab West subsequently split by cone and quartering (Campos-M and Campos-C., 2017) to obtain subsamples allowing XRF, particle size and QEMSCAN analysis. There was not enough sample from the PI-SWERL exhaust sample at Huab East for XRF analysis and only QEMSCAN was performed on this exhaust sample. The three sample types are hereafter referred to as “Surface”, “PI-SWERL” and “BSNE” samples.

273 **Table 1 Sample details from the Surface, BSNE and PI-SWERL exhaust.**

Sample ID	Sample location	Sample height relative to surface (m)	Collection start and end date
Surface E	East	-0.02 to 0	18/09/2015
PI-SWERL E	PI-SWERL transect Huab 1 and 2	0	18/09/2015
BSNE E**	East (H2)	0.89	07/07/2013-01/08/2013
Surface W	West	-0.02 to 0	18/09/2015
PI-SWERL W	PI-SWERL transect Huab 7	0	18/09/2015
BSNE W	West (H7)	0.89	09/07/2013-03/08/2013

274 The BSNE sample locations at H2 and H7 correspond with those described by Dansie et al.
275 (2017a).

276

XRF

The elemental composition of all surface and BSNE samples and the West Huab PI-SWERL sample were analysed with a Spectroscout energy-dispersive X-ray Fluorescence (XRF) analyser (SPECTRO Analytical Instruments, Kleve, Germany). There was insufficient material for the second PI-SWERL (East) sample to be analysed. The XRF was calibrated with a certified standard GBW07312 (National Research Center for CRMs, Beijing, China) for which technical concentrations were obtained from NOAA Technical memorandum NOS ORCA 68 (1992). This analysis was performed to validate the auto-SEM-EDS (QEMSCAN) results.

Auto-SEM-EDS analysis (QEMSCAN)

The samples were analysed using a FEG QEMSCAN 650F and accompanying software, iDiscover^{TM} with the aim of determining the size, mineralogy and shape of the individual particles. A description of QEMSCAN principles can be found in Gottlieb et al., (2000) and Goodall et al., (2005). The bulk surface samples were screened over a 250 and 63 µm sieve. The two fractions <63 µm and 63-250 µm were analysed separately, but the results are aggregated when referring to Surface East or Surface West samples. The PI-SWERL and BSNE samples did not consist of particles greater than 250 µm. A subsample was further split by rotary micro-splitter to obtain approximately 0.2 g of material for QEMSCAN analysis and subsequently mounted in resin. The samples were mixed with graphite in a 2:1 (sample: graphite) ratio to ensure maximum dispersion and to aid with electron conductivity. This mixture was then added to resin and stirred vigorously in a figure of eight pattern to ensure complete mixing and random orientation of all particles. The sample moulds were placed in a vacuum chamber for 10 minutes and then again for 5 minutes, breaking the vacuum in between to release any trapped air bubbles. The moulds were cured overnight in a pressure pot and the blocks removed for polishing the next day. The blocks were polished in a series of grinding and polishing steps with a final polishing cloth size of 1 µm. The grinding and polishing

sequence were as follows: grinding with Struers MD-Piano 1200, followed by polishing with MD-Largo 6 µm cloth, MD-Dur 3 µm and finishing off with MD-Nap 1 µm cloth. The blocks were inspected with an optical microscope at each stage to ensure there are no plucked or cracked grains and to ensure a smooth surface. The blocks were carbon coated and placed in a vacuum cupboard overnight before analysis. It is important to acknowledge that the sample preparation would result in alteration of the sampled sediment, but all the samples underwent the same protocols to allow for the comparison of the results from the different sampling approaches. The sample mounting underwent extensive testing to determine the most appropriate methodology for the comparative purposes of this study (see details in supplementary material, section S1). The surface samples also underwent screening as part of the sample preparation to represent the wind-erodible fraction as in previous studies (e.g. Bhattachan et al., 2015; von Holdt and Eckardt, 2017; Wang et al., 2005; Guieu et al., 2002, Shi et al., 2011).

Samples were scanned at 2 µm/pixel for a minimum of 2 hours which yielded approximately 10,000 – 60,000 individual particle images per sample. This provided a large enough number of randomly oriented particles for a comparative assessment of particle size. All particles were categorised into the following size fractions: <5, 5-10, 10-20, 20-63, 63-125, 125-150, 150-350 and >350 µm using the calculated equivalent circle diameter (ECD) of the measurement of the flat, cross-sections of the particle (Little, 2016; Ralph and Kurzydlowski, 1997). Shape characteristics were determined on the flat cross-sections of the particles according to the classification system used by Little et al. (2015) using measures of roundness and aspect ratio.

The identification of mineral phases with the QEMSCAN is not fully automated and still requires considerable input from the user of the instrument. The user must create a SIP (Species Identification Protocol) list which classifies the minerals based on the BSE and EDS elemental

concentrations for each pixel. The classification of the measured spectra has to be evaluated by using several criteria including elemental ranges and ratios (Little, 2016).

Results

Particle size distributions

A total of 171,104 particles were scanned for all six samples from Huab West and East providing the size, mineralogy, elemental composition and shape of each particle scanned at 2 µm/ pixel resolution. The particle-size distributions based on the total area of pixels in each size bin of the bulk surface, PI-SWERL, and BSNE samples for both sites are different for the three sampling methods (Figure 4a and Table 2). This is especially evident for the East site, with the bulk Surface and BSNE showing a maximum in the 20-63 µm size bin and the PI-SWERL a maximum in the 10-20 µm bin. In addition, the proportions of the sample in each size category differ within the smaller size bins (Table 2), with a much smaller percentage of the sample falling in the <20 µm size class for the Surface and BSNE East sample. Almost all of the particles from the PI-SWERL samples were less than 100 µm (98.5 % at the East site and 100 % at the West site). The PI-SWERL sample at the East site had a small fraction of particles in the coarser bins (0.41 % in 100–125 µm and 1.07 % in 150–350 µm). At Huab West, all the samples have a maximum in the 20-63 µm bin, similar to the Surface and BSNE East samples. The PI-SWERL West sample had a significantly larger proportion within the 10-20 µm bin compared to the other two methods. In comparison, the BSNE West sample had the largest proportion of <10 µm fraction (Table 2) at this site. The number size distribution (Figure 4b) illustrates the predominance of the <10 µm fraction for the PI-SWERL and surface samples at the East site (greater than 95%), whereas the BSNE sample only has 63.7% <10 µm and 96.1% <63 µm. The samples from the West site all have a number size distribution of at least 98% <63 µm, with the BSNE having the largest number of particles in the smallest size class

350 (38% <5 μm). The number distribution of the PI-SWERL East and BSNE West samples follow
351 the same trend (Figure 4b). As additional information, the PI-SWERL emission fluxes for all
352 sites tested in the Huab are given in supplementary section S2 as boxplots per site. The emission
353 flux results for the individual runs for the PI-SWERL samples in the East and West are also
354 presented in supplementary section S2.

355

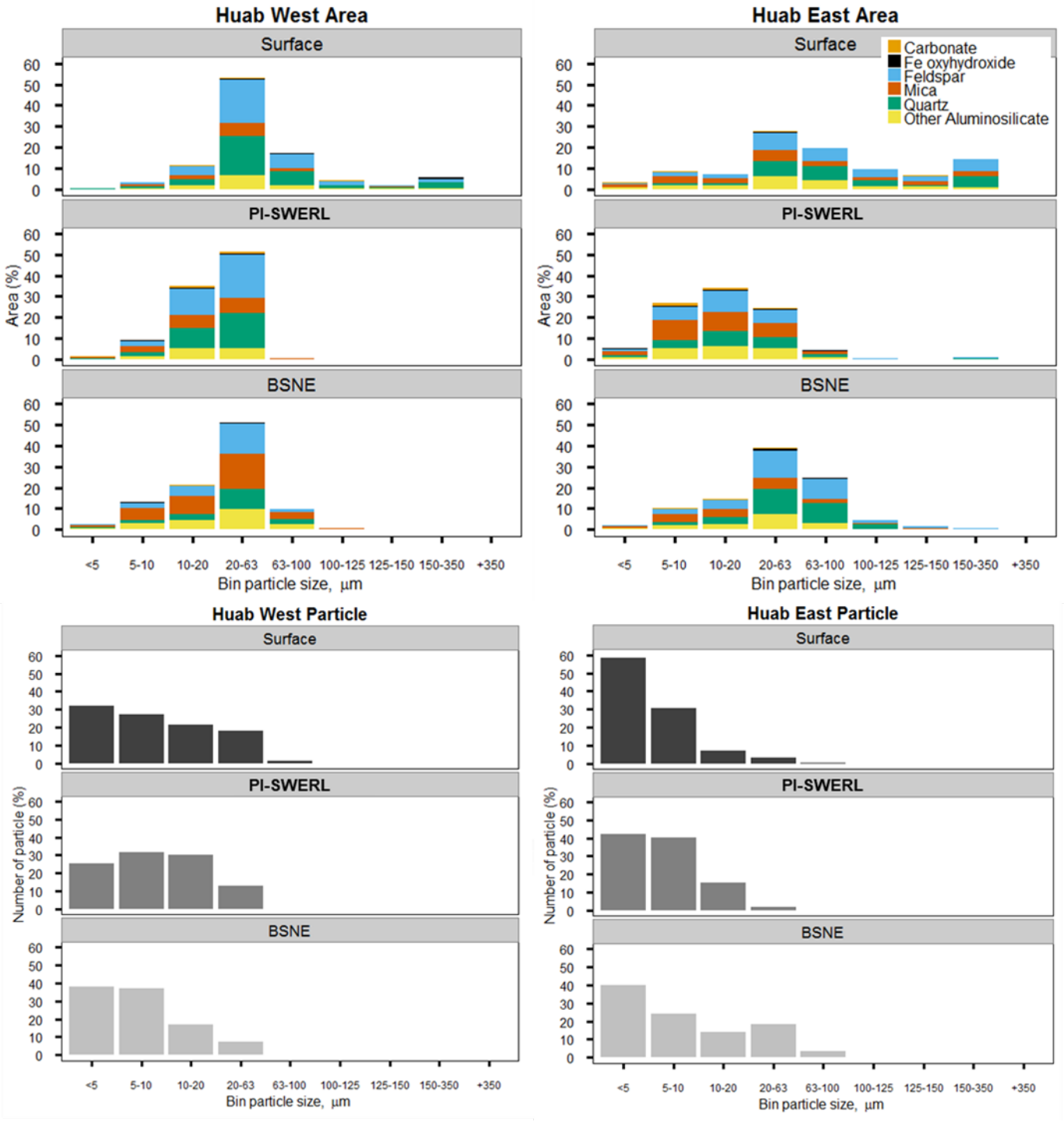

356

357 **Figure 4 Comparison of particle size distribution based on a) area, and b) number of particles**
358 **from the QEMSCAN analysis. Particles are placed in size bins based on the equivalent circle**
359 **diameter (ECD) of each measured particle.**

360

Table 2 Cumulative percentages of samples in selected size fractions based on QEMSCAN analysis

	<5 µm	<10 µm	<20 µm	<63 µm	<100 µm
Surface West	0.7	4.3	16.2	70.8	88.4
PI-SWERL West	1.4	11.0	47.1	99.4	100.0
BSNE West	2.8	16.5	38.1	90.3	99.5
Surface East	3.3	12.2	19.7	48.6	68.9
PI-SWERL East	5.9	33.9	69.2	94.3	98.5
BSNE East	2.3	13.1	28.4	68.2	93.2

Mineralogical comparison

The sampled dust from the BSNEs and the PI-SWERL and bulk surface fine sediments consist of a mixture of minerals consisting of predominantly feldspar; quartz; mica; other aluminosilicates such as epidote, chlorite, amphibole and pyroxene; iron oxyhydroxides; titanium minerals; carbonates and clay minerals. The mineralogy of the samples shows varying combinations of these minerals, but the contribution of mica to the BSNE West and PI-SWERL East sample is markedly different from the other samples. The mica makes up the largest proportion of all the size fractions in these two samples (Figure 4a, Figure 5). The ability of the BSNEs to catch mica differed between the two sites with the BSNE East not being effective at trapping mica in the <20 µm fraction. In contrast, the BSNE West trapped proportionately more mica than collected from the PI-SWERL or as represented in the surface sediments. Mica was the dominant mineral in the <5 and 5-10 µm size fractions for all the samples, but contributed more to the total size class mineralogy for the BSNE W (7.0%) and PI-SWERL East (12.0%), compared to the other samples (1.3-4.6%). The PI-SWERL East sample also had

379 a higher carbonate content in the 5-10 μm fraction compared to the trend for the total size
380 distribution.

381 The quantity of mica showed large variations as indicated by the total mineralogy (Figure 5).
382 Mica comprised the largest contribution for the PI-SWERL East and BSNE West samples. The
383 mineral distribution for these two samples was very similar, including the other
384 aluminosilicates, possibly suggesting that the material captured by BSNE West originated from
385 the surfaces found further upstream in the river towards the east. The BSNE East sample was
386 relatively depleted in mica compared to the surface and PI-SWERL sample, indicating that less
387 mica was being trapped by this sampler. The BSNE captured sediments in the west were damp
388 (possibly due to frequent fog-events) when it was collected, which could explain why this
389 BSNE successfully trapped both finer particles and more mica. In contrast, the BSNE East
390 sampler would be less likely to experience wet conditions given its location further inland
391 (Eckardt et al., 2013). The degree of dispersion is an important consideration in any analysis
392 of the size and composition of dust particles. The sediments in the present analysis cannot be
393 regarded as fully dispersed because some agglomerations were present in all the samples. This
394 occurred despite dispersion procedures during sample preparation that resulted in the
395 disaggregation of most clusters. The number of agglomerated particles was determined by
396 measuring the number of pixels within the particle that were classified as background, i.e. no
397 mineral data recorded for that pixel. The percentages of agglomerated particles were
398 sufficiently low for all the samples (<3.9%), except for the Surface East (63-250 μm) fraction
399 which had 6.3% agglomerations (see supplementary section S3). A distinction should be made
400 between agglomerations of finer particles (Figure 6 BSNE W) and finer particles cemented
401 onto larger particles (Figure 6 BSNE E). The particle images in Figure 6 were taken from a
402 top-mounted sample, with undispersed aggregates (not used in this analysis but for image
403 purposes only). Any agglomerations of finer particles should be regarded as having the

potential to produce finer particles, despite being classified in a larger size class. All the samples underwent the same particle mounting procedure and agitation and are therefore regarded as suitably comparable.

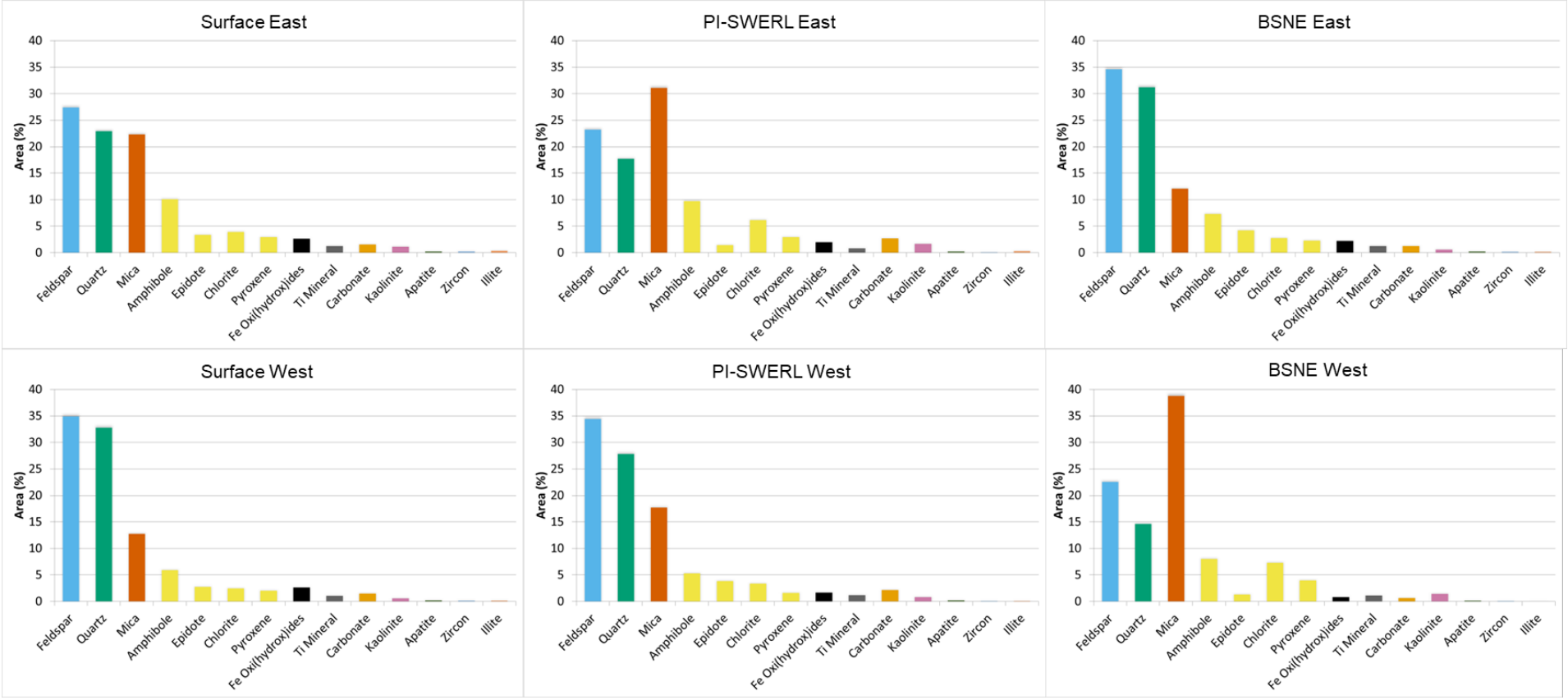

Figure 5 The total mineral distribution for each sample. Feldspar, quartz and mica are the predominant minerals. The PI-SWERL East sample is dominated by mica compared to the less abundant quantity in the BSNE East sample. In contrast, the BSNE West sample is dominated by mica,

with much less mica in the corresponding PI-SWERL West sample. The other aluminosilicates for the BSNE West and PI-SWERL East show a similar trend. The carbonates and Fe oxyhydroxides are less abundant in the BSNE West compared to the PI-SWERL East sample

415

416

417

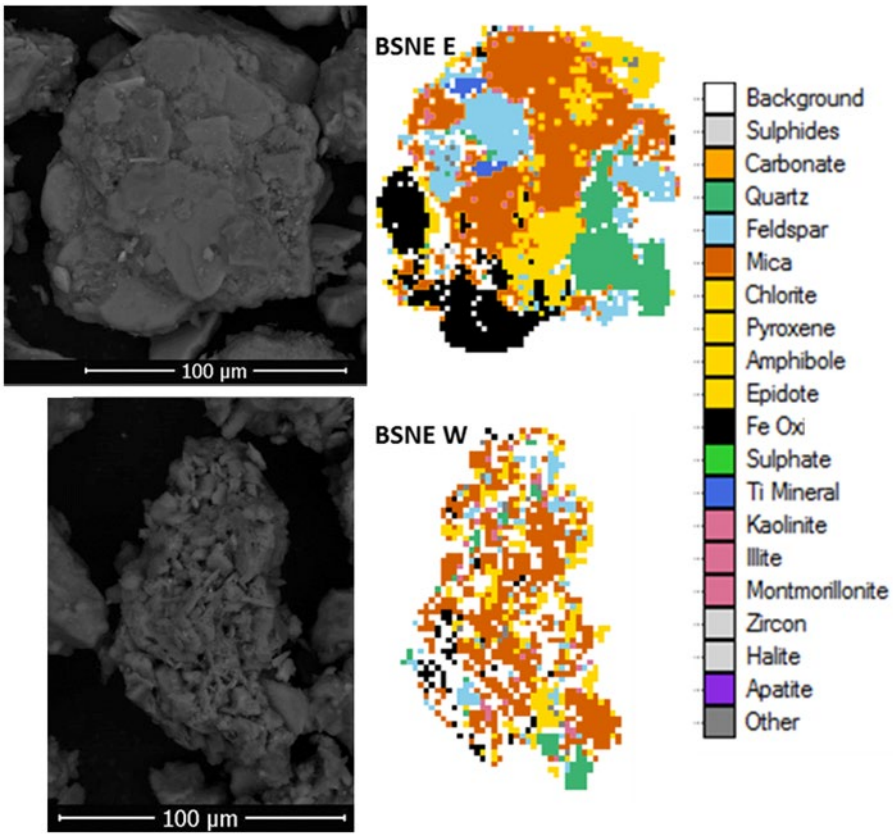

Figure 6 SEM image and false colour image of particles consisting of various minerals. BSNE E is an example of a larger particle with fine particles cemented to it and the BSNE W particle is an agglomeration of finer particles with a high proportion of background (blank) pixels identified within the particle image. These images and mineralogy scans were produced from the top-mounted samples, whereas all other results are based on the resin mounted samples.

Elemental distributions

The elemental residence of Fe, Ca and P within the size classes indicates that these elements are concentrated in the wind-erodible fraction (Figure 7). According to our analysis, the Fe is mainly associated with Fe oxyhydroxides, mica and other aluminosilicates, with minor amounts associated with feldspar, titanium minerals and the clays of kaolinite (0.001-0.005% Fe associated with kaolinite as percentage of total Fe oxyhydroxides) and illite (0.001-0.007% Fe associated with illite as percentage of total Fe oxyhydroxides). The Fe oxyhydroxides consist mostly of goethite (α-FeO(OH)) and a goethite-clay interface. The Fe associated with the clay minerals as part of this study has concentrations of 0.01% for BSNE West, 0.008% from the PI-SWERL East and 0.008% for Surface East, whereas the remaining samples have concentrations of 0.003-0.004%. Calcium is predominantly associated with the Fe and Ca-rich aluminosilicates, feldspar and carbonates predominantly as calcite. Minor amounts of Ca are present in titanium minerals, apatite and clay minerals. Only the BSNE West and PI-SWERL East samples have Ca present in the form of sulphate, predominantly as gypsum. Phosphorous was only associated with apatite. In their study of the nutrient availability in sediments, Dansie et al. (2017b) suggested that most of the P contained in the ephemeral rivers in the Namib is derived from the geology (as apatite) and potentially accumulated in sediments in the lower reaches of the ephemeral rivers as they flow through the desert due to the decrease in vegetation to utilise this nutrient.

447

448

449

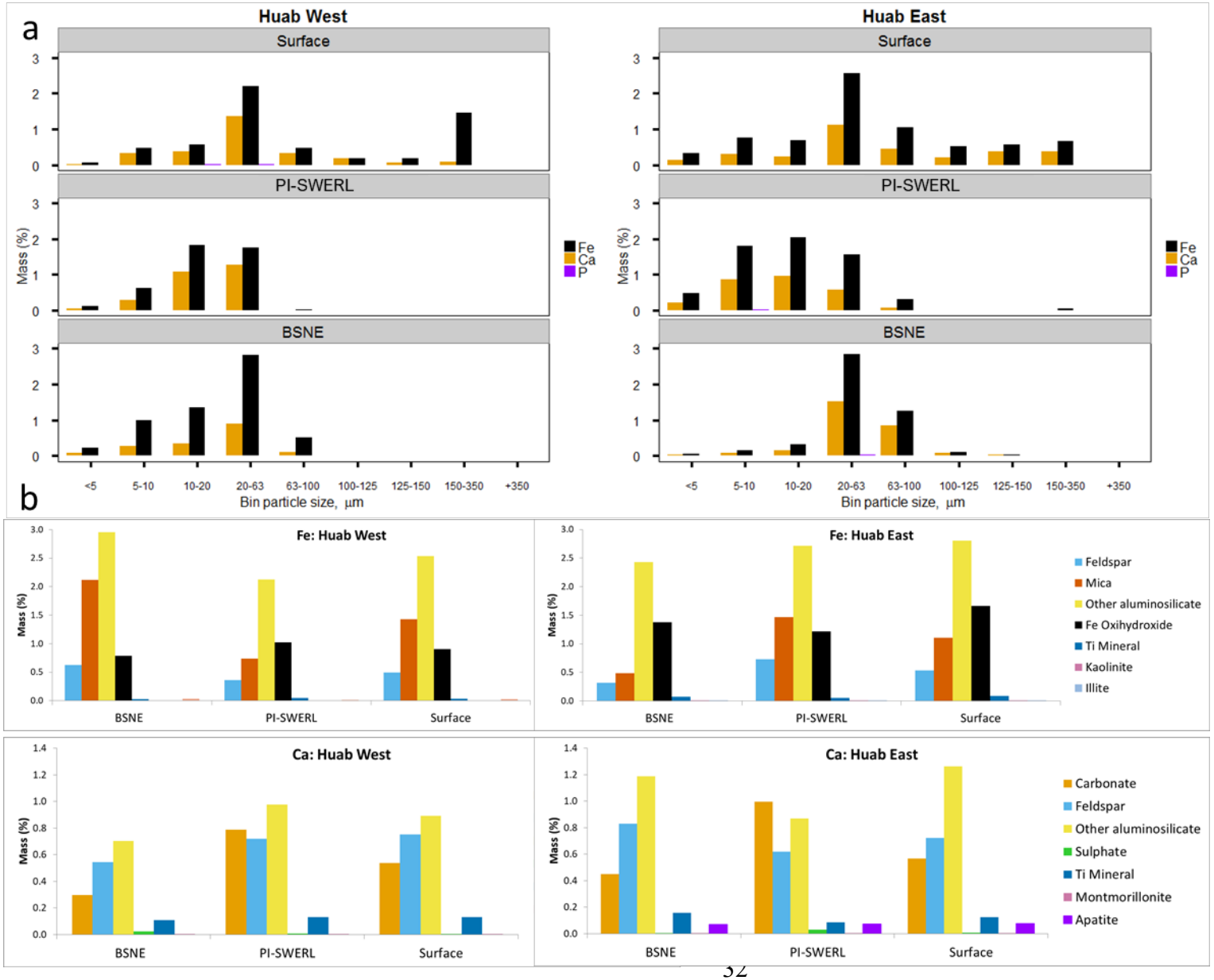
a
Huab West
Huab East
Surface
PI-SWERL
BSNE
Mass (%)
Fe
Ca
P
<5
5-10
10-20
20-63
63-100
100-125
125-150
150-350
+350
Bin particle size, µm
b
Fe: Huab West
Fe: Huab East
Feldspar
Mica
Other aluminosilicate
Fe Oxihydroxide
Ti Mineral
Kaolinite
Illite
BSNE
PI-SWERL
Surface
Ca: Huab West
Ca: Huab East
Carbonate
Feldspar
Other aluminosilicate
Sulphate
Ti Mineral
Montmorillonite
Apatite

450

Figure 7 Element residence of Fe, Ca and P within size classes (a) and Fe and Ca within different minerals present in all size classes (b). The (mass %) refers to the percentage of the element in the given size fraction or mineral phase as a percentage of the total sample

Shape characteristics

The shape analysis classifies most particles for all sampling methods and both sites as sub-angular to angular based on the number of particles classified according to the roundness criteria for the >5 μm fraction (Figure 8). The BSNE West sampled predominantly angular and subangular particles concentrated in the 5–20 μm size fraction. The shape distribution of the PI-SWERL West sample is very similar to the BSNE in the same area. The BSNE East displayed a larger angular component in the 20–63 μm range, greater than that seen in either the surface or the PI-SWERL sample at the same site. All the samples have a maximum frequency in the sub-angular roundness class (0.4-0.6). The elongated and angular class (<0.2) is dominated by platy micas (evident in Figure 8b).

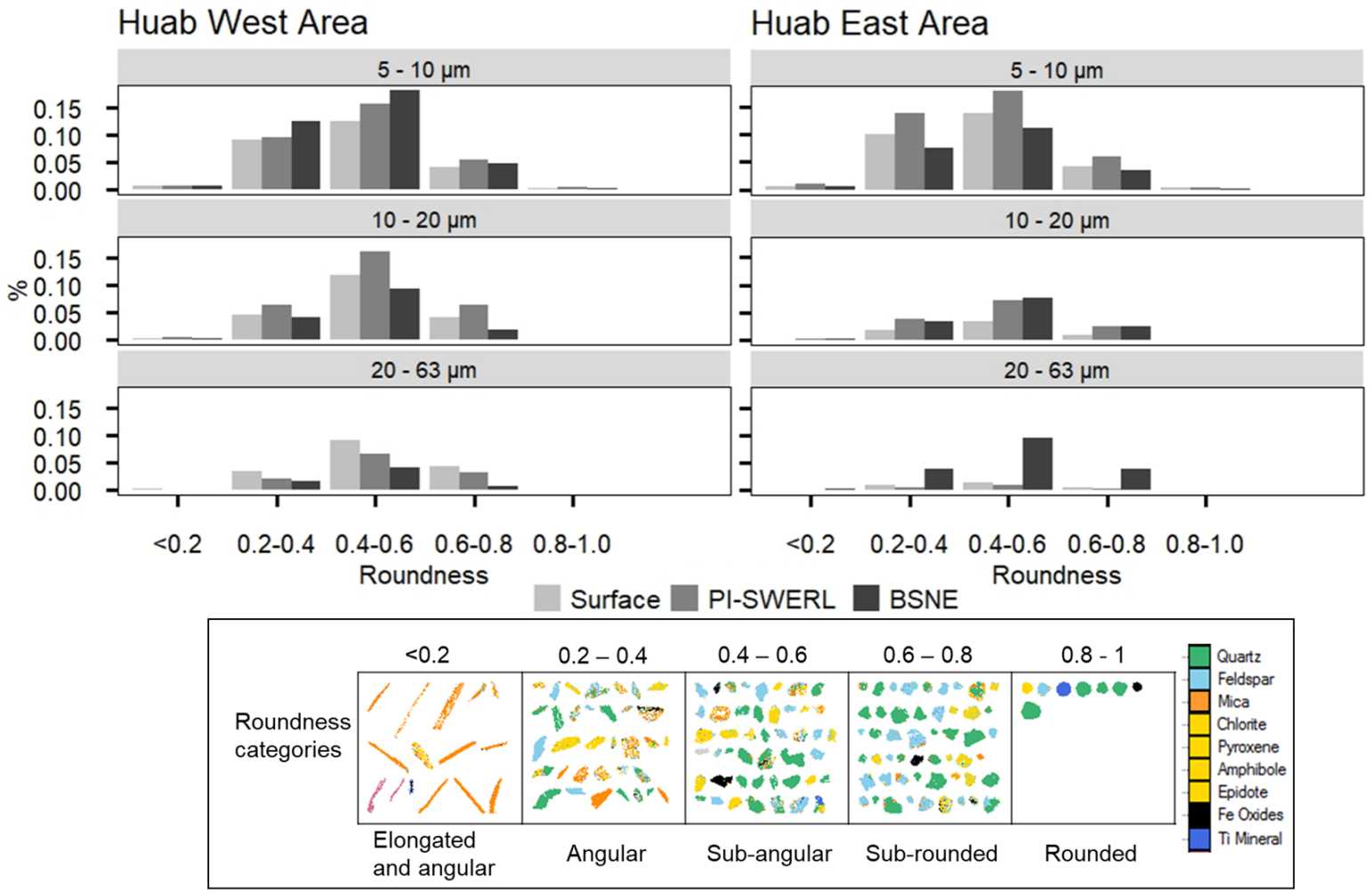
Huab West Area
Huab East Area
5 - 10 µm
10 - 20 µm
20 - 63 µm
%
0.15
0.10
0.05
0.00
<0.2
0.2-0.4
0.4-0.6
0.6-0.8
0.8-1.0
Roundness
Surface
PI-SWERL
BSNE
Roundness categories
<0.2
0.2 – 0.4
0.4 – 0.6
0.6 – 0.8
0.8 - 1
Elongated and angular
Angular
Sub-angular
Sub-rounded
Rounded
Quartz
Feldspar
Mica
Chlorite
Pyroxene
Amphibole
Epidote
Fe Oxides
Ti Mineral

Figure 8 a) Roundness distributions for the three sampling methods at the two sites for the 5–63 µm fraction. Most of the particles are classified in the angular to sub-angular classes. b) The 20-63 µm fraction for BSNE East sample. Roundness can only be determined for >5 µm sizes given the scanning resolution of 2 µm/pixel used for this study (effective resolution of 2.75 µm).

Discussion

The three different sampling methods tested here produced a range of different characterisations of aeolian dust (emitted or potentially emitted) as collected within a known source of emission in the Huab River valley of the Namib Desert. Analysis of the upper 0.02 m surface samples as a proxy for emitted dust resulted in less representation of the <20 µm fraction relative to the emitted dust sample generated by the PI-SWERL (Table 2). At both the East and West sites in the Huab, the PI-SWERL had higher quantities of dust in the <20 µm fraction due to the preferential entrainment of finer particles (Table 2). The East PI-SWERL sample also preferentially entrained more mica compared to what is present in the surface sample for the <20 µm fraction (Figure 4). The ability to obtain physical samples of entrained dust from the PI-SWERL (Wang et al. 2017) provides the opportunity to directly compare the surface sediments with what is entrained from that surface, in addition to the <10 µm real time dust flux measurements. Using a surface-sediment sample could potentially provide a coarser representation of emitted dust, whereas the PI-SWERL would appear to provide a finer size distribution more representative of emitted particles.

The <10 µm fractions of particle size in the BSNE samples had distributions quite different to those of the PI-SWERL samples. The East PI-SWERL captured more sample in the fractions <10 µm (33.9 %, Table 2), in relation to the comparable BSNE sample (13.1 %). In contrast, the West PI-SWERL captured less sample in the same <10 µm fraction (11.0 %) compared to the BSNE sample (16.5 %). The trend reverses for the 10-63 µm, where the BSNE consists of less in these size fractions than the PI-SWERL sample. The larger quantity of the finest fractions trapped by the BSNE might be regarded as contrary to what would be expected as the BSNE sampler is known to be inefficient at trapping dust in the finest fractions, being most efficient for particles of >30 µm (Sow et al., 2006; Mendez et al., 2011) with efficiencies of between 10% and 40% (Mendez et al., 2016; Shao et al., 1993; Sharrat et al., 2007) reported

497 for the <10 μm fraction. Dansie et al. (2017a) who sampled in the same region over a different
498 time period similarly found that the BSNE West had the smallest median diameter (26.8-27.1
499 μm) of all the sampling sites in the Huab, suggesting that this result was due to a combination
500 of fluvial and aeolian processes in sorting dust-sized sediment. Ephemeral fluvial flows would
501 likely produce deposition of progressively finer material downstream, while dust emitted from
502 upstream source areas and in transport would become finer at the point of sampling due to
503 gravitational settling of the larger particles during transport. However, it is possible that the
504 ability of the BSNE West sampler to trap the finer fraction is also due to the prevailing
505 environmental conditions at this site. The Huab West site near the coast experiences high
506 atmospheric humidity and experiences predominantly south-westerly onshore winds. An
507 increased ability to retain fine particles within this sampler could be due to the moisture
508 creating a physical crust of the trapped sediments at the bottom of the sampler, preventing re-
509 entrainment of the sample, or alternatively, the wetting of the sediments changing the
510 aerodynamics of the sampler and thereby increasing its ability to trap fines. The BSNE has a
511 simple, cheap and robust design, but moisture is a problem when sampling windblown
512 sediment leading to some researchers suggesting the construction of rain hoods to protect the
513 samples in the traps (Shao et al., 1993). The effects of fog precipitation and inland sea spray
514 are, however, more difficult to control. Any significant influence on the likelihood of trapping
515 the finest dust fractions or the modification of the aerodynamics of the sampler (such as
516 isokinetic characteristics) due to environmental conditions would result in biased and
517 inconsistent representations of windblown sediments.

518 The predominance of the proportion of finer particles (<63 μm) in the PI-SWERL samples may
519 also be due to interaction between entrained particles and the fast-rotating metal annular ring
520 of the device, with collision resulting in a more fully dispersed particle size distribution (Shao,
521 2004). One consequence of this interaction suggested by Vickery (2014), is that additional

522 abrasion and rounding of particles could result in higher dust concentration than naturally
523 occurring by emission from the surface while additionally changing the particle characteristics.
524 The abrasion and rounding of particles were not found to be the case in the present study as the
525 surface and PI-SWERL sample roundness values follow the same trend across all size fractions.
526 (Figure 8a). The friction velocity used for testing by Vickery (2014) was significantly higher
527 (5300rpm) than the present study (3300rpm), which could result in more abrasion and alteration
528 of the particles in that study.

529 The Huab sediments sampled by all three methods consisted of particles made up of a mixture
530 of minerals derived from the weathering of the local metamorphic geology and subsequent
531 transport of sediment within the catchment. The combination of the different rock types within
532 the catchment makes for a rich mixture of minerals reflected in the sediments derived from
533 these rocks. The internally mixed mineralogy of these particles is similar to that found for
534 example by Falkovich et al. (2001), who reported that only 10% of the particles in their study
535 collected on filter membranes at the eastern coast of the Mediterranean and originating in North
536 Africa, were composed of a single mineral. The individual particle analysis of the three
537 sampling approaches shows appreciable differences resulting in variations in the particle size
538 distributions and composition of the particles. Such divergent representations of what is
539 potentially emitted have important consequences when drawing conclusions from an analysis
540 of the characteristics of sampled dust at the emission source or using the representation of dust
541 in modelling efforts (Krueger et al., 2004; Fitzgerald et al., 2015).

542 Despite the differences in the representation of the dust sampled by the three methods assessed
543 here, the individual particle analysis still provides important detailed information about the
544 potential ecological and atmospheric impacts of dust from the Huab source area. Modelling
545 studies generally assume spherical particles (e.g. Lui et al., 2016) and ideal optical properties
546 based on the chemical composition of the dust (Kandler et al., 2007). The high mica content

547 and mixed mineralogy, fine particle sizes and angular shape of the particles sampled in the
548 present study all represent a departure from an idealised attempt at particle characterisation. In
549 addition, the mica particles appear to have surface coatings of finer particles cemented onto
550 them (Figure 6). The weathering of iron-rich biotite, as well as clay minerals adhered on these
551 mica particles could result in an increased concentration of Fe associated with these particles
552 that can travel further distances than more spherical particles of equivalent size. The ability of
553 coarser, platy particles to travel further was noted by Friese et al. (2016), who argued that the
554 coarse shoulder (approx. 100 to 250 μm) of their samples trapped at almost 1000 km offshore
555 consisted of large platy particles as a result of their ability to travel further than spherical
556 particles for a given wind speed.

557 Nutrients contained in the dust, especially bioavailable Fe, have been an important aspect of
558 dust research (Jickells and Moore, 2015; Mahowald et al., 2005). The Fe in the Huab samples
559 is concentrated in the wind erodible fraction as Fe oxyhydroxides, within the aluminosilicates,
560 the titanium minerals and to a lesser extent the clay minerals (Figure 7b). There is still
561 considerable uncertainty regarding the reactivity and bioavailability of the Fe in the different
562 mineral phases within dust. Journet et al. (2008) proposed that the Fe in the clay minerals is
563 the most soluble and as a result more bioavailable compared to the other mineral associations.
564 The concentration of Fe associated with clay minerals in the different samples highlight the
565 similarity between sediments from the BSNE west and Huab east sites, but also reveal
566 difference over orders of magnitude between the sampling approaches. Dansie et al., (2017a)
567 reported bioavailable Fe concentrations in the BSNE windblown sediments of 0.00055% and
568 0.00071% within the surface sediments, values that are an order of magnitude lower than the
569 Fe associated with the clays. Helping to account for the fact that clay particles are more iron-
570 rich, Moskowitz et al. (2016) found that a large proportion of the ferric oxide minerals occurs
571 as nanosized particles associated with clay minerals and that many of these nanoparticles were

572 on the surfaces of the clay minerals. Furthermore, aside from Fe presence, solubility of Fe
573 could also be influenced by the presence of other mineral phases. For example, Hettiarachchi
574 et al. (2018) reported an increase in Fe solubility with an increase in TiO_2, also present in the
575 sediments sampled here (Figure 5) and associated with Fe (Figure 7). The association of this
576 bioavailable Fe with the various mineral components of the dust needs further investigation
577 and the dust characteristics of the Namib ephemeral rivers (including the Huab) present an ideal
578 study site. Furthermore, a combination of sampling methods, including the PI-SWERL exhaust
579 sampling, with a computer-controlled SEM individual particle size analysis could make an
580 important contribution to this field of research. The benefits of combining a passive sampler
581 with an automated single-particle analysis has also been suggested by Waza et al., (2019).

582 In addition, the inclusion of optical particle counters (OPS) such as by Bachelder et al, (2019)
583 would provide a means to further improve field sampling and characterisation of emitted dust.
584 The inefficiency of the BSNE sampler in trapping fine particles (Shao et al., 1993; Sharratt et
585 al., 2007; Sow et al., 2006), confirmed by the comparison of methods in the present study, may
586 result in an under-estimation of the nutrient content of emitted dust, especially the bioavailable
587 Fe content delivered to the ocean, as investigated by Dansie et al. (2017a).

588 ## Conclusion

589 Different sampling techniques could result in a misrepresentation of the influence of the dust,
590 including a potential underestimation of the nutrient content contained within the sediments.
591 Three different methods, representing aeolian dust samples, are compared (emitted or
592 potentially emitted) at a single emission source. The methods produce variable characteristics
593 for a range of fundamental dust properties. The size distributions, mineralogy and shape of the
594 particles show appreciable differences for each of the three sampling approaches. BSNEs are
595 known to under-perform at trapping particle sizes <30 μm, especially in higher wind speeds,

596 and this can result in an underestimation of the quantity of emitted dust in this size fraction.
597 Our data suggest that one BSNE consisted of proportionally less <20 µm compared to the PI-
598 SWERL sample, while a second BSNE comparison characterised a greater <10 µm size
599 fraction than the PI-SWERL, and less in the specific 10-20 µm fraction. These nuances indicate
600 important implications for accurate determination of the suspended PSD, and in this case,
601 indicate a role for the high humidity in proximity to the coast as preferentially trapping <10 um
602 material. Similarly, our findings show that using a surface sample to represent dust emission
603 potential could also result in an underestimation of fine fractions, specifically <20 µm. The
604 bulk surface sample and BSNE potentially underrepresents the fines, whereas the PI-SWERL
605 potentially results in an over representation of the fines.

606 All three methods used in the Huab valley dust source area confirm the complex mixed
607 mineralogy of the particles. Most particles consist of different combinations of minerals with
608 some important differences found in different size fractions, especially the mica The analysis
609 also highlighted the size fraction with the highest concentration of iron to be present as part of
610 the aluminosilicate minerals, with lesser amounts as oxides and a limited association with clay
611 minerals (<0.01 %). The iron is most abundant in the 20 – 63 µm fraction for the Surface and
612 BSNE samples, whereas in the PI-SWERL east the iron is concentrated in the 5 to 63 µm
613 fraction and in the PI-SWERL west found predominantly in the 10 – 63 µm size range. Most
614 of the particles >5 µm were classified as angular to sub-angular. This complex mineralogy
615 needs to be considered when referring to different size bins, their shape, composition and
616 optical properties of the particles for use in models. The representation of mineralogy will differ
617 depending on the chosen method with bulk surface sampling and dust trapping (BSNE)
618 resulting in a potential under-estimation of important elements, such as iron, and a potential
619 over representation from a PI-SWERL exhaust sample.

Novel sampling from the PI-SWERL exhaust has been performed successfully as part of this study, but the possibility of abrasion of particles by the rotating ring remains uncertain, especially in terms of its implications for characterising shape. The determination of fluid and particle flow inside the PI-SWERL would potentially provide a fuller appreciation of the results from this instrument, something that might be achieved through application of Particle Image Velocimeter (PIV) technology to the internal flow field (Johnson et al., 2010). The ability provided by the PI-SWERL, to test the emission potential of a surface at a set friction velocity and obtain a physical sample of the entrained sediments, provides an opportunity to formulate valuable characterisations of dust emission at source from specific surfaces. Our findings stress that environmental conditions at the time of PI-SWERL testing (especially moisture-related) can represent a significant influence on the nature of the emitted dust and these need to be recognised for systematic use of the PI-SWERL in a role as a dust generator. Different sampling approaches will provide different representations of emitted dust and should be taken into consideration when evaluating particle size and mineral (or nutrient) composition of samples.

Acknowledgements

This research was funded by the National Research Foundation in South Africa as part of research project UID 89120. We thank the Ministry of Environment and Tourism for their support and assistance for the duration of this research. This research was conducted under MET permit number 2076/2015. Thank you to the Dust Observation DO4 Models project for making the BSNE samples available and for the use of the PI-SWERL. We also thank Gaynor Yorath, Lorraine Nkemba and Megan Becker from the Centre for Minerals Research at the University of Cape Town for assistance with the sample preparation and running of the QEMSCAN.

644 **References**

645 Atkinson, J., Murray, B., Woodhouse, M. *et al.* The importance of feldspar for ice nucleation by
646 mineral dust in mixed-phase clouds. Nature 498, pp.355–358 (2013),
647 https://doi.org/10.1038/nature12278.

648 Bachelder, J., Cadieux, M., Liu-Kang, C., Lambert, P., Filoche, A., Galhardi, J.A., Hadioui, M.,
649 Chaput, A., Bastien-Thibault, M.P., Wilkinson, K.J. and King, J., 2020. Chemical and microphysical
650 properties of wind-blown dust near an actively retreating glacier in Yukon, Canada. Aerosol Sci and
651 Technol, 54(1), pp.2-20, doi: 10.1080/02786826.2019.1676394.

652 Bacon, S. N., E. V. McDonald, R. Amit, Y. Enzel, and O. Crouvi (2011), Total suspended particulate
653 matter emissions at high friction velocities from desert landforms, J. Geophys. Res., 116, F03019,
654 doi:10.1029/2011JF001965.

655 Bhattachan, A., D'Odorico, P. and Okin, G.S., 2015. Biogeochemistry of dust sources in Southern
656 Africa. J. Arid Environ., 117, pp.18-27, https://doi.org/10.1016/j.jaridenv.2015.02.013.

657 Campos-M, M. and Campos-C, R., 2017. Applications of quartering method in soils and foods. Int. J.
658 Eng. Res. Appl, 7(1), pp.35-39, doi: 10.9790/9622-0701023539.

659 Claquin, T., Schulz, M. and Balkanski, Y.J., 1999. Modeling the mineralogy of atmospheric dust
660 sources. J. Geophys. Res., 104(D18), pp.22243-22256, https://doi.org/10.1029/1999JD900416.

661 Cui, M., Lu, H., Wiggs, G.F., Etyemezian, V., Sweeney, M.R. and Xu, Z., 2019. Quantifying the
662 effect of geomorphology on aeolian dust emission potential in northern China. Earth Surf. Process.
663 Landf., 44(14), pp.2872-2884, https://doi.org/10.1002/esp.4714.

664 Dansie, A.P., Wiggs, G.F.S., Thomas, D.S.G. and Washington, R., 2017a. Measurements of
665 windblown dust characteristics and ocean fertilization potential: The ephemeral river valleys of
666 Namibia. Aeolian Res, 29, pp.30-41, https://doi.org/10.1016/j.aeolia.2017.08.002.

667 Dansie, A.P., Thomas, D.S.G., Wiggs, G.F.S. and Munkittrick, K.R., 2018. Spatial variability of
668 ocean fertilizing nutrients in the dust-emitting ephemeral river catchments of Namibia. Earth Surf.
669 Process. Landf., 43(3), pp.563-578, doi: 10.1002/esp.4207.

670 Deboudt, K., P. Flament, M. Choël, A. Gloter, S. Sobanska, and C. Colliex (2010), Mixing state of
671 aerosols and direct observation of carbonaceous and marine coatings on African dust by individual
672 particle analysis, J. Geophys. Res., 115, D24207, doi:10.1029/2010JD013921.

673 Eckardt, F.D., Soderberg, K., Coop, L.J., Muller, A.A., Vickery, K.J., Grandin, R.D., Jack, C.,
674 Kapalanga, T.S. and Henschel, J., 2013. The nature of moisture at Gobabeb, in the central Namib
675 Desert. J. Arid Environ., 93, pp.7-19, https://doi.org/10.1016/j.jaridenv.2012.01.011.

676 Engelbrecht, J.P., McDonald, E.V., Gillies, J.A., Jayanty, R.K.M., Casuccio, G. and Gertler, A.W.,
677 2009. Characterizing mineral dusts and other aerosols from the Middle East—part 1: ambient
678 sampling. Inhal. Toxicol., 21(4), pp.297-326, doi: 10.1080/08958370802464273.

679 Engelbrecht, J.P., Moosmüller, H., Pincock, S., Jayanty, R.K.M., Lersch, T. and Casuccio, G., 2016.
680 Mineralogical, chemical, morphological, and optical interrelationships of mineral dust re-
681 suspensions. Atmospheric Chem. Phys., 16(17), pp.10809-10830. https://doi.org/10.5194/acp-16-
682 10809-2016.

683 Etyemezian, V., Nikolich, G., Ahonen, S., Pitchford, M., Sweeney, M., Purcell, R., Gillies, J. &
684 Kuhns, H. 2007. The Portable In Situ Wind Erosion Laboratory (PI-SWERL): A new method to
685 measure PM10 windblown dust properties and potential for emissions. Atmos. Environ., 41(18),
686 pp.3789–3796, https://doi.org/10.1016/j.atmosenv.2007.01.018.

687 Etyemezian, V., Gillies, J.A., Shinoda, M., Nikolich, G., King, J. and Bardis, A.R., 2014. Accounting
688 for surface roughness on measurements conducted with PI-SWERL: Evaluation of a subjective visual
689 approach and a photogrammetric technique. Aeolian Res., 13, pp.35-50,
690 https://doi.org/10.1016/j.aeolia.2014.03.002.

691 Falkovich, A.H., Ganor, E., Levin, Z., Formenti, P. and Rudich, Y., 2001. Chemical and
692 mineralogical analysis of individual mineral dust particles. J. Geophys. Res., 106(D16), pp.18029-
693 18036, https://doi.org/10.1029/2000JD900430.

694 Fitzgerald, E., Ault, A.P., Zauscher, M.D., Mayol-Bracero, O.L. and Prather, K.A., 2015. Comparison
695 of the mixing state of long-range transported Asian and African mineral dust. Atmos. Environ., 115,
696 pp.19-25, https://doi.org/10.1016/j.atmosenv.2015.04.031.

697 Formenti, P., Elbert, W., Maenhaut, W., Haywood, J. and Andreae, M.O., 2003. Chemical
698 composition of mineral dust aerosol during the Saharan Dust Experiment (SHADE) airborne
699 campaign in the Cape Verde region, September 2000. J. Geophys. Res., 108(D18), 8576,
700 doi:10.1029/2002JD002648.

701 Formenti, P., Schütz, L., Balkanski, Y., Desboeufs, K., Ebert, M., Kandler, K., Petzold, A.,
702 Scheuvens, D., Weinbruch, S. and Zhang, D., 2011. Recent progress in understanding physical and
703 chemical properties of African and Asian mineral dust. Atmospheric Chem. Phys., 11 (16), pp.8231-
704 8256, https://doi.org/10.5194/acp-11-8231-2011.

705 Friese, C.A., van der Does, M., Merkel, U., Iversen, M.H., Fischer, G. and Stuut, J.B.W., 2016.
706 Environmental factors controlling the seasonal variability in particle size distribution of modern
707 Saharan dust deposited off Cape Blanc. Aeolian Res., 22, pp.165-179,
708 https://doi.org/10.1016/j.aeolia.2016.04.005.

709 Fryberger, S.G., 1979. Dune forms and wind regimes. In: McKee, E.D. (Ed.), A study of Global Sand
710 Seas. USGS Professional paper 1052, pp. 137-169.

711 Fryrear, D.W., 1986. A field dust sampler. Journal of Soil and Water Conservation, 41(2), pp.117-
712 120.

713 Gillette, D.A., Fryrear, D.W., Gill, T.E., Ley, T., Cahill, T.A. and Gearhart, E.A., 1997. Relation of
714 vertical flux of particles smaller than 10 μm to total aeolian horizontal mass flux at Owens Lake. J.
715 Geophys. Res., 102(D22), pp.26009-26015, https://doi.org/10.1029/97JD02252.

716 Ginoux, P., 2003. Effects of nonsphericity on mineral dust modeling. J. Geophys. Res., 108(D2),
717 4052, doi:10.1029/2002JD002516.

718 Goodall, W.R., Scales, P.J. and Butcher, A.R., 2005. The use of QEMSCAN and diagnostic leaching
719 in the characterisation of visible gold in complex ores. Miner. Eng., 18(8), pp.877-886,
720 https://doi.org/10.1016/j.mineng.2005.01.018.

721 Goossens, D. and Buck, B., 2009. Dust emission by off-road driving: Experiments on 17 arid soil
722 types, Nevada, USA. Geomorphology, 107(3), pp.118-138,
723 https://doi.org/10.1016/j.geomorph.2008.12.001.

724 Goossens, D. and Buck, B., 2012. Can BSNE (Big Spring Number Eight) samplers be used to
725 measure PM10, respirable dust, PM2.5 and PM1.0? Aeolian Res., 5, pp.43-49,
726 https://doi.org/10.1016/j.aeolia.2012.03.002.

727 Gottlieb, P., Wilkie, G., Sutherland, D., Ho-Tun, E., Suthers, S., Perera, K., Jenkins, B., Spencer, S.,
728 Butcher, A. and Rayner, J., 2000. Using quantitative electron microscopy for process mineralogy
729 applications. JoM, 52(4), pp.24-25, https://doi.org/10.1007/s11837-000-0126-9.

730 Guieu, C., Loÿe-Pilot, M.D., Ridame, C. and Thomas, C., 2002. Chemical characterization of the
731 Saharan dust end-member: Some biogeochemical implications for the western Mediterranean Sea. J.
732 Geophys. Res., 107(D15), pp.ACH-5, doi:10.1029/2001JD000582.

733 Hahnenberger, M. and Perry, K.D., 2015. Chemical comparison of dust and soil from the Sevier Dry
734 Lake, UT, USA. Atmos. Environ., 113, pp.90-97, https://doi.org/10.1016/j.atmosenv.2015.04.054.

735 Hayton, S., Nelson, C.S., Ricketts, B.D., Cooke, S. and Wedd, M.W., 2001. Effect of mica on
736 particle-size analyses using the laser diffraction technique. J. Sediment. Res., 71(3), pp.507-509,
737 https://doi.org/10.1306/2DC4095B-0E47-11D7-8643000102C1865D.

738 Hettiarachchi, E., Reynolds, R.L., Goldstein, H.L., Moskowitz, B. and Rubasinghege, G., 2018. Iron
739 dissolution and speciation in atmospheric mineral dust: Metal-metal synergistic and antagonistic
740 effects. Atmos. Environ., 187, pp.417-423, https://doi.org/10.1016/j.atmosenv.2018.06.010.

741 Hojati, S., Khademi, H., Cano, A.F. and Landi, A., 2012. Characteristics of dust deposited along a
742 transect between central Iran and the Zagros Mountains. Catena, 88(1), pp.27-36,
743 https://doi.org/10.1016/j.catena.2011.09.002.

744 Jeong, G.Y., 2008. Bulk and single-particle mineralogy of Asian dust and a comparison with its
745 source soils. J. Geophys. Res., 113(D02208), https://doi.org/10.1029/2007JD008606.

746 Jerram, D., Mountney, N., Holzförster, F. and Stollhofen, H., 1999. Internal stratigraphic relationships
747 in the Etendeka Group in the Huab Basin, NW Namibia: understanding the onset of flood
748 volcanism. J. Geodyn., 28(4), pp.393-418, https://doi.org/10.1016/S0264-3707(99)00018-6.

749 Jerram, D.A., Mountney, N.P., Howell, J.A., Long, D. and Stollhofen, H., 2000. Death of a sand sea:
750 an active aeolian erg systematically buried by the Etendeka flood basalts of NW Namibia. J. Geol.
751 Soc. London., 157(3), pp.513-516, https://doi.org/10.1144/jgs.157.3.513.

752 Jickells, T.D., An, Z.S., Andersen, K.K., Baker, A.R., Bergametti, G., Brooks, N., Cao, J.J., Boyd,
753 P.W., Duce, R.A., Hunter, K.A. and Kawahata, H., 2005. Global iron connections between desert
754 dust, ocean biogeochemistry, and climate. Science, 308(5718), pp.67-71, doi:
755 10.1126/science.1105959.

756 Jickells, T. and Moore, C.M., 2015. The importance of atmospheric deposition for ocean
757 productivity. Annu. Rev. Ecol. Evol. Syst., 46, pp.481-501, doi: 10.1146/annurev-ecolsys-112414-
758 054118.

759 Johnson, B., Leishman, J.G. and Sydney, A., 2010. Investigation of Sediment Entrainment Using
760 Dual-Phase, High-Speed Particle Image Velocimetry. J. Am. Helicopter Soc., 55(4), pp.42003-42003,
761 https://doi.org/10.4050/JAHS.55.042003.

762 Journet, E., Desboeufs, K.V., Caquineau, S. and Colin, J.L., 2008. Mineralogy as a critical factor of
763 dust iron solubility. Geophys. Res. Lett., 35 (L07805), doi:10.1029/2007GL031589.

764 Journet, E., Balkanski, Y. and Harrison, S.P., 2014. A new data set of soil mineralogy for dust-cycle
765 modeling. Atmospheric Chem. Phys., 14(8), pp.3801-3816, https://doi.org/10.5194/acp-14-3801-
766 2014.

767 Kalashnikova, O.V. and Sokolik, I.N., 2002. Importance of shapes and compositions of wind-blown
768 dust particles for remote sensing at solar wavelengths. Geophys. Res. Lett., 29(10),
769 doi:10.1029/2002GL014947.

770 Kandler, K., Benker, N., Bundke, U., Cuevas, E., Ebert, M., Knippertz, P., Rodríguez, S., Schütz, L.
771 and Weinbruch, S., 2007. Chemical composition and complex refractive index of Saharan Mineral
772 Dust at Izana, Tenerife (Spain) derived by electron microscopy. Atmos. Environ., 41(37), pp.8058-
773 8074, https://doi.org/10.1016/j.atmosenv.2007.06.047.

774 Kandler, K., Schütz, L., Deutscher, C., Ebert, M., Hofmann, H., Jäckel, S., Jaenicke, R., Knippertz, P.,
775 Lieke, K., Massling, A. and Petzold, A., 2009. Size distribution, mass concentration, chemical and
776 mineralogical composition and derived optical parameters of the boundary layer aerosol at Tinfou,
777 Morocco, during SAMUM 2006, Tellus B Chem. Phys. Meteorol., 61(1), pp.32-50,
778 https://doi.org/10.1111/j.1600-0889.2008.00385.x.

779 Kok, J.F., 2011a. Does the size distribution of mineral dust aerosols depend on the wind speed at
780 emission? Atmospheric Chem. Phys., 11(19), pp.10149-10156, https://doi.org/10.5194/acp-11-10149-
781 2011.

782 Kok, J.F., 2011b. A scaling theory for the size distribution of emitted dust aerosols suggests climate
783 models underestimate the size of the global dust cycle. Proc. Natl. Acad. Sci. U.S.A., 108(3),
784 pp.1016-1021, doi: 10.1073/pnas.1014798108.

785 Kok, J.F., Parteli, E.J., Michaels, T.I. and Karam, D.B., 2012. The physics of wind-blown sand and
786 dust. Rep. Prog. Phys., 75(10), p.106901, https://doi.org/10.1088/0034-4885/75/10/106901.

787 Knippertz P. and Stuut JB.W. 2014. Introduction. In: Knippertz P., Stuut JB. (eds) Mineral Dust.
788 Springer, Dordrecht, https://doi.org/10.1007/978-94-017-8978-3_1.

789 Krueger, B.J., Grassian, V.H., Laskin, A. and Cowin, J.P., 2003. The transformation of solid
790 atmospheric particles into liquid droplets through heterogeneous chemistry: Laboratory insights into
791 the processing of calcium containing mineral dust aerosol in the troposphere. Geophys. Res.
792 Lett., 30(3), 1148, doi:10.1029/2002GL016563.

793 Krueger, B.J., Grassian, V.H., Cowin, J.P. and Laskin, A., 2004. Heterogeneous chemistry of
794 individual mineral dust particles from different dust source regions: the importance of particle
795 mineralogy. Atmos. Environ., 38(36), pp.6253-6261, https://doi.org/10.1016/j.atmosenv.2004.07.010.

796 Lafon, S., Sokolik, I.N., Rajot, J.L., Caquineau, S. and Gaudichet, A., 2006. Characterization of iron
797 oxides in mineral dust aerosols: Implications for light absorption. J. Geophys. Res., 111, D21207,
798 doi:10.1029/2005JD007016.

799 Laskin, A., Iedema, M.J., Ichkovich, A., Graber, E.R., Taraniuk, I. and Rudich, Y., 2005. Direct
800 observation of completely processed calcium carbonate dust particles. Faraday Discuss., 130, pp.453-
801 468, doi: 10.1039/B417366J.

802 Little, L. 2016. The development and demonstration of a practical methodology for fine particle shape
803 characterisation in minerals processing, PhD thesis, University of Cape Town, Cape Town, South
804 Africa (August).

805 Little, L., Becker, M., Wiese, J. and Mainza, A.N., 2015. Auto-SEM particle shape characterisation:
806 Investigating fine grinding of UG2 ore. Miner. Eng., 82, pp.92-100,
807 https://doi.org/10.1016/j.mineng.2015.03.021.

808 Mahowald, N., 2011. Aerosol indirect effect on biogeochemical cycles and
809 climate. Science, 334(6057), pp.794-796, doi: 10.1126/science.1207374.

810 Mahowald, N.M., Baker, A.R., Bergametti, G., Brooks, N., Duce, R.A., Jickells, T.D., Kubilay, N.,
811 Prospero, J.M. and Tegen, I., 2005. Atmospheric global dust cycle and iron inputs to the
812 ocean. Global Biogeochem. Cycles, 19, GB4025, doi:10.1029/2004GB002402.

Mahowald, N., Albani, S., Kok, J.F., Engelstaeder, S., Scanza, R., Ward, D.S. and Flanner, M.G., 2014. The size distribution of desert dust aerosols and its impact on the Earth system. Aeolian Res., 15, pp.53-71, https://doi.org/10.1016/j.aeolia.2013.09.002.

McTainsh, G. and Strong, C., 2007. The role of aeolian dust in ecosystems. Geomorphology, 89(1), pp.39-54, https://doi.org/10.1016/j.geomorph.2006.07.028.

Mendez, M.J., Funk, R. and Buschiazzo, D.E., 2011. Field wind erosion measurements with big spring number eight (BSNE) and modified wilson and cook (MWAC) samplers. Geomorphology, 129(1), pp.43-48, https://doi.org/10.1016/j.geomorph.2011.01.011.

Mendez, M.J., Funk, R. and Buschiazzo, D.E., 2016. Efficiency of big spring number eight (BSNE) and modified Wilson and Cook (MWAC) samplers to collect PM10, PM2. 5 and PM1. Aeolian Res., 21, pp.37-44, https://doi.org/10.1016/j.aeolia.2016.02.003.

Moskowitz, B.M., Reynolds, R.L., Goldstein, H.L., Berquó, T.S., Kokaly, R.F. and Bristow, C.S., 2016. Iron oxide minerals in dust-source sediments from the Bodélé Depression, Chad: Implications for radiative properties and Fe bioavailability of dust plumes from the Sahara. Aeolian Res., 22, pp.93-106, https://doi.org/10.1016/j.aeolia.2016.07.001.

Muhs D.R., Prospero J.M., Baddock M.C. and Gill T.E. 2014. Identifying sources of aeolian mineral dust: present and past. In: Stuut J.-B. and Knippertz P. (Eds.), Mineral dust – a key player in the Earth system. Springer, Berlin. pp.51-74, https://doi.org/10.1007/978-94-017-8978-3_3.

Nickovic, S., Vukovic, A., Vujadinovic, M., Djurdjevic, V. and Pejanovic, G., 2012. High-resolution mineralogical database of dust-productive soils for atmospheric dust modeling. Atmospheric Chem. Phys., 12(2), pp.845-855, https://doi.org/10.5194/acp-12-845-2012.

NOAA Technical Memorandum NOS ORCA 68, 1992. Standard and reference materials for marine science (3rd edition), NOAA, Rockville, pp 325-327. Available online at: https://repository.library.noaa.gov/view/noaa/2881/noaa_2881_DS1.pdf?

837 Nousiainen, T., 2009. Optical modeling of mineral dust particles: A review. J. Quant. Spectrosc.
838 Radiat. Transfer, 110(14), pp.1261-1279, https://doi.org/10.1016/j.jqsrt.2009.03.002.

839 Ralph, B. and Kurzydłowski, K.J., 1997. Methods for the characterization of grain size. Mater.
840 Charact., 38(3), pp.177-185, https://doi.org/10.1016/S1044-5803(97)00042-9.

841 Rashki, A., Eriksson, P.G., Rautenbach, C.D.W., Kaskaoutis, D.G., Grote, W. and Dykstra, J., 2013.
842 Assessment of chemical and mineralogical characteristics of airborne dust in the Sistan region,
843 Iran. Chemosphere, 90(2), pp.227-236, https://doi.org/10.1016/j.chemosphere.2012.06.059.

844 Reheis, M.C., Budahn, J.R., Lamothe, P.J. and Reynolds, R.L., 2009. Compositions of modern dust
845 and surface sediments in the Desert Southwest, United States. J. Geophys. Res., 114, F01028,
846 doi:10.1029/2008JF001009.

847 Reid, E.A., Reid, J.S., Meier, M.M., Dunlap, M.R., Cliff, S.S., Broumas, A., Perry, K. and Maring,
848 H., 2003. Characterization of African dust transported to Puerto Rico by individual particle and size
849 segregated bulk analysis. J. Geophys. Res., 108, 8591, doi:10.1029/2002JD002935, D19.

850 Reynolds, R.L., Yount, J.C., Reheis, M., Goldstein, H., Chavez, P., Fulton, R., Whitney, J., Fuller, C.
851 and Forester, R.M., 2007. Dust emission from wet and dry playas in the Mojave Desert,
852 USA. Earth Surf. Process. Landf., 32, pp.1811-1827, https://doi.org/10.1002/esp.1515.

853 Ryder, C.L., Highwood, E.J., Rosenberg, P.D., Trembath, J., Brooke, J.K., Bart, M., Dean, A.,
854 Crosier, J., Dorsey, J., Brindley, H. and Banks, J., 2013. Optical properties of Saharan dust aerosol
855 and contribution from the coarse mode as measured during the Fennec 2011 aircraft
856 campaign. Atmospheric Chem. Phys., 13(1), pp.303-325, https://doi.org/10.5194/acp-13-303-2013.

857 Shao, Y., 2004. Simplification of a dust emission scheme and comparison with data. J. Geophys. Res.,
858 109, D10202, doi:10.1029/2003JD004372.

859 Shao, Y., McTainsh, G.H., Leys, J.F. and Raupach, M.R., 1993. Efficiencies of sediment samplers for
860 wind erosion measurement. Soil Res., 31(4), pp.519-532, https://doi.org/10.1071/SR9930519.

Shao, Y., Wyrwoll, K.H., Chappell, A., Huang, J., Lin, Z., McTainsh, G.H., Mikami, M., Tanaka, T.Y., Wang, X. and Yoon, S., 2011a. Dust cycle: An emerging core theme in Earth system science. Aeolian Res., 2(4), pp.181-204, https://doi.org/10.1016/j.aeolia.2011.02.001.

Shao, Y., Ishizuka, M., Mikami, M. and Leys, J.F., 2011b. Parameterization of size-resolved dust emission and validation with measurements. J. Geophys. Res., 116, D08203, doi:10.1029/2010JD014527.

Sharratt, B., Feng, G. and Wendling, L., 2007. Loss of soil and PM10 from agricultural fields associated with high winds on the Columbia Plateau. Earth Surf. Process. Landf., 32(4), pp.621-630, https://doi.org/10.1002/esp.1425.

Shi, Z., Shao, L., Jones, T.P. and Lu, S., 2005. Microscopy and mineralogy of airborne particles collected during severe dust storm episodes in Beijing, China. J. Geophys. Res., 110, D01303, doi:10.1029/2004JD005073.

Shi, Z., Krom, M.D., Bonneville, S., Baker, A.R., Bristow, C., Drake, N., Mann, G., Carslaw, K., McQuaid, J.B., Jickells, T. and Benning, L.G., 2011. Influence of chemical weathering and aging of iron oxides on the potential iron solubility of Saharan dust during simulated atmospheric processing. Global Biogeochem. Cycles, 25(GB2010), doi:10.1029/2010GB003837.

Sokolik, I.N. and Toon, O.B., 1999. Incorporation of mineralogical composition into models of the radiative properties of mineral aerosol from UV to IR wavelengths. J. Geophys. Res., 104(D8), pp.9423-9444, doi:10.1029/1998JD200048.

Sow, M., Goossens, D. and Rajot, J.L., 2006. Calibration of the MDCO dust collector and of four versions of the inverted frisbee dust deposition sampler. Geomorphology, 82(3-4), pp.360-375, https://doi.org/10.1016/j.geomorph.2006.05.013.

Speirs, J.C., McGowan, H.A. and Neil, D.T., 2008. Polar eolian sand transport: grain characteristics determined by an automated scanning electron microscope (QEMSCAN®). Arct. Antarct. Alp. Res., 40(4), pp.731-743, doi: 10.1657/1523-0430(07-029)[SPEIRS]2.0.CO;2.

886 Stout, J.E., 2007. Simultaneous observations of the critical aeolian threshold of two surfaces.
887 Geomorphology 85 (1–2), pp.3–16, http://dx.doi.org/10.1016/j.geomorph.2006.
888 03.034.

889 Sullivan, R.C., Moore, M.J.K., Petters, M.D., Kreidenweis, S.M., Roberts, G.C. and Prather, K.A.,
890 2009. Effect of chemical mixing state on the hygroscopicity and cloud nucleation properties of
891 calcium mineral dust particles. Atmospheric Chem. Phys., 9(10), pp..3303-3316,
892 https://doi.org/10.5194/acp-9-3303-2009.

893 Sweeney, M., Etyemezian, V., Macpherson, T., Nickling, W., Gillies, J., Nikolich, G., & McDonald,
894 E., 2008. Comparison of PI-SWERL with dust emission measurements from a straight-line field wind
895 tunnel. J. Geophys. Res., 113(F01012), pp.1–12, doi:10.1029/2007JF000830.

896 Sweeney, M. R., McDonald, E. V., & Etyemezian, V., 2011. Quantifying dust emissions from desert
897 landforms, eastern Mojave Desert, USA. Geomorphology, 135(1–2), pp.21–34.

898 Sweeney, M.R., Zlotnik, V.A., Joeckel, R.M. and Stout, J.E., 2016. Geomorphic and hydrologic
899 controls of dust emissions during drought from Yellow Lake playa, West Texas, USA. J. Arid
900 Environ., 133, pp.37-46, https://doi.org/10.1016/j.jaridenv.2016.05.007.

901 Thomas, D.S., Durcan, J.A., Dansie, A. and Wiggs, G.F., 2017. Holocene fluvial valley fill sources of
902 atmospheric mineral dust in the Skeleton Coast, Namibia. Earth Surf. Process. Landf., 42(12),
903 pp.1884-1894, doi: 10.1002/esp.4151.

904 Trapp, J.M., Millero, F.J. and Prospero, J.M., 2010. Temporal variability of the elemental composition
905 of African dust measured in trade wind aerosols at Barbados and Miami. Mar. Chem., 120(1), pp.71-
906 82, https://doi.org/10.1016/j.marchem.2008.10.004.

907 van der Does, M., Korte, L. F., Munday, C. I., Brummer, G. A., & Stuut, J. W. 2016. Particle size
908 traces modern saharan dust transport and deposition across the equatorial north atlantic. Atmospheric
909 Chem. Phys., 16(21), pp.13697-13710, https://doi.org/10.5194/acp-16-13697-2016.

910 Van Pelt R.S., Baddock M.C, Zobeck T.M., D'Odorico P., Ravi S. and Bhattachan A. 2017. Total
911 vertical sediment flux and PM10 emissions from disturbed Chihuahuan Desert surfaces. Geoderma,
912 293, pp.19-25, https://doi.org/10.1016/j.geoderma.2017.01.031.

913 Vickery, K. 2014. The nature of pan sediments: A case study on dust supply from the Makgadikgadi
914 pans, Botswana. PhD Thesis. University of Cape Town.

915 Vickery, K.J., Eckardt, F.D. and Bryant, R.G., 2013. A sub-basin scale dust plume source frequency
916 inventory for southern Africa, 2005–2008. Geophys. Res. Lett., 40(19), pp.5274-5279,
917 doi:10.1002/grl.50968.

918 Vickery, K. and Eckardt, F., 2020. A closer look at mineral aerosol emissions from the Makgadikgadi
919 Pans, Botswana, using automated SEM-EDS (QEMSCAN®). S. Afr. Geogr. J.,
920 doi:10.1080/03736245.2020.1824805.

921 von Holdt, J.R. and Eckardt, F.D., 2017. Dust activity and surface sediment characteristics of the
922 dustiest river in southern Africa: the Kuiseb River, Central Namib. S. Afr. Geogr. J., 100:1, pp.104-
923 121, doi: 10.1080/03736245.2017.1339627

924 von Holdt, J.R., Eckardt, F.D., Wiggs, G.F.S. 2017. Landsat identifies aeolian dust emission dynamics
925 at the landform scale. Remote Sens. Environ., 198, pp.229–243,
926 https://doi.org/10.1016/j.rse.2017.06.010.

927 von Holdt, J.R., Eckardt, F.D., Baddock, M.C., Wiggs, G.F.S. 2019. Assessing landscape dust
928 emission schemes using combined ground-based process and remote sensing data. J. Geophys. Res.,
929 124, pp.1080-1098, https://doi.org/10.1029/2018JF004713.

930 Wang, X., Dong, Z., Yan, P., Yang, Z. and Hu, Z., 2005. Surface sample collection and dust source
931 analysis in northwestern China. Catena, 59(1), pp.35-53, https://doi.org/10.1016/j.catena.2004.05.009.

932 Wang, X., Chow, J.C., Kohl, S.D., Yatavelli, L.N.R., Percy, K.E., Legge, A.H. and Watson, J.G.,
933 2015. Wind erosion potential for fugitive dust sources in the Athabasca Oil Sands Region. Aeolian
934 Res., 18, pp.121-134, https://doi.org/10.1016/j.aeolia.2015.07.004.

Wang, X., Lang, L., Hua, T., Zhang, C. and Li, H., 2018. The effects of sorting by aeolian processes on the geochemical characteristics of surface materials: a wind tunnel experiment. Front. Earth Sci., 12(1), pp.86-94, https://doi.org/10.1007/s11707-017-0619-2.

Warren, A., Chappell, A., Todd, M.C., Bristow, C., Drake, N., Engelstaedter, S., Martins, V., M'bainayel, S. and Washington, R., 2007. Dust-raising in the dustiest place on earth. Geomorphology, 92(1), pp.25-37, https://doi.org/10.1016/j.geomorph.2007.02.007.

Waza, A., Schneiders, K., May, J., Rodríguez, S., Epple, B. and Kandler, K., 2019. Field comparison of dry deposition samplers for collection of atmospheric mineral dust: results from single-particle characterization. Atmos. Meas. Tech., (12), pp.6647-6665, https://doi.org/10.5194/amt-12-6647-2019.

Yang, X., Liu, Y., Li, C., Song, Y., Zhu, H. and Jin, X., 2007. Rare earth elements of aeolian deposits in Northern China and their implications for determining the provenance of dust storms in Beijing. Geomorphology, 87(4), pp.365-377, https://doi.org/10.1016/j.geomorph.2006.10.004.

Zhang, J., Wu, Y., Liu, C.L., Shen, Z.B., Yu, Z.G. and Zhang, Y., 2001. Aerosol characters from the desert region of Northwest China and the Yellow Sea in spring and summer: observations at Minqin, Qingdao, and Qianliyan in 1995–1996. Atmos. Environ., 35(29), pp.5007-5018, https://doi.org/10.1016/S1352-2310(01)00269-2.

Zhuang, G., Guo, J., Yuan, H. and Zhao, C., 2001. The compositions, sources, and size distribution of the dust storm from China in spring of 2000 and its impact on the global environment. Chin.Sci.Bull., 46(11), pp.895-900, https://doi.org/10.1007/BF02900460.